The performance of BM@N spectrometer

BMN collaboration

February 2023

1 Introduction

BM@N (baryonic matter at Nuclotron) is the first experiment ~~operational~~ at the ion-accelerating complex Nuclotron/NICA, studying interactions of relativistic ion beams of heavy ions with fixed targets [1] in the energy range ~~of high densities of baryonic matter [2]~~. At ~~the Nuclotron~~ energies, the density of nucleons in a fireball created by two colliding heavy nuclei is 3-4 times higher than the nuclear saturation density[3]. In addition, these energies are high enough to study strange mesons and (multi)-strange hyperons produced in nucleus-nucleus collisions close to the kinematic threshold [4, 5]. The primary goal of the experiment is to constrain parameters of the equation of state (EoS) of high-density nuclear matter. Studies of the excitation function of strange particle production below and near to the kinematical threshold make it possible to distinguish hard behaviour of the EoS from the soft one [6].

The Nuclotron will provide the experiment with beams of a variety of particles, from protons to gold ions, with kinetic energy in the range from 1 to 6 GeV/nucleon for light ions with Z/A ratio of ~ 0.5 and up to 4.5 GeV/nucleon for heavy ions with Z/A ratio of ~ 0.4.

The BM@N detector is a forward spectrometer covering the pseudorapidity range $1.6 \leq \eta \leq 4.4$. Schematic view of the BM@N setup is shown in Fig. 1. ~~The description of the spectrometer subsystems is organised in a "downstream beam" order.~~ The details for all subsystems are given in a corresponding sections below.

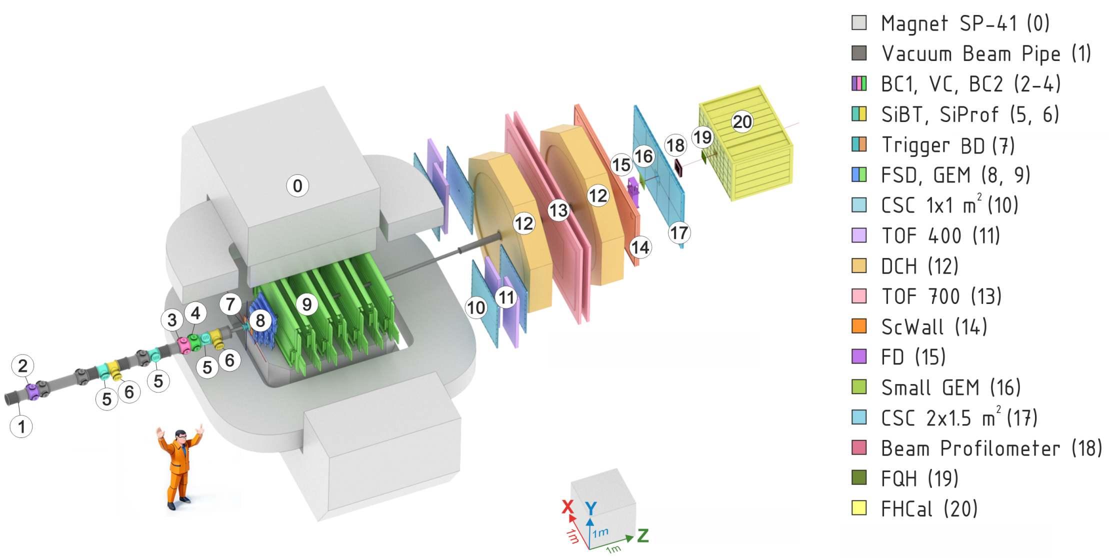

Figure 1: Schematic view of BM@N setup in RUN8.

2 Beamline

2.1 Beam transport

The BM@N experiment is part of the NICA complex (see Fig. 2), located on the extracted beam from the Nuclotron in the target hall.

Electronic string source of the highly-charged ions "KRION-6", provides heavy ions of Au^{31+} (up to $2 * 10^9$ per pulse with a pulse repetition rate of 10 Hz) and delivers them into the HILac.

The main tasks of the booster are as follows:

- accumulation of ions at an injection energy of $2.5 * 10^9$ $^{197}Au^{31+}$ ions;
- effective acceleration of incompletely stripped ions, which is possible due to the ultrahigh vacuum in the beam chamber;
- formation of the required phase volume of the beam using an ECS at an energy of 65 MeV/n;
- acceleration of heavy ions to the energy required for their efficient stripping;
- fast (single-lap) extraction of the accelerated beam for its injection into the Nuclotron.

The Nuclotron SC proton synchrotron has three operation modes:

- Acceleration of heavy ions for storage in the collider.
- Acceleration of polarized protons and deuterons for feeding the collider.
- Acceleration of both polarized and unpolarized protons and deuterons and heavy ions for internal target experiments or slow extraction to fixed target experiments.

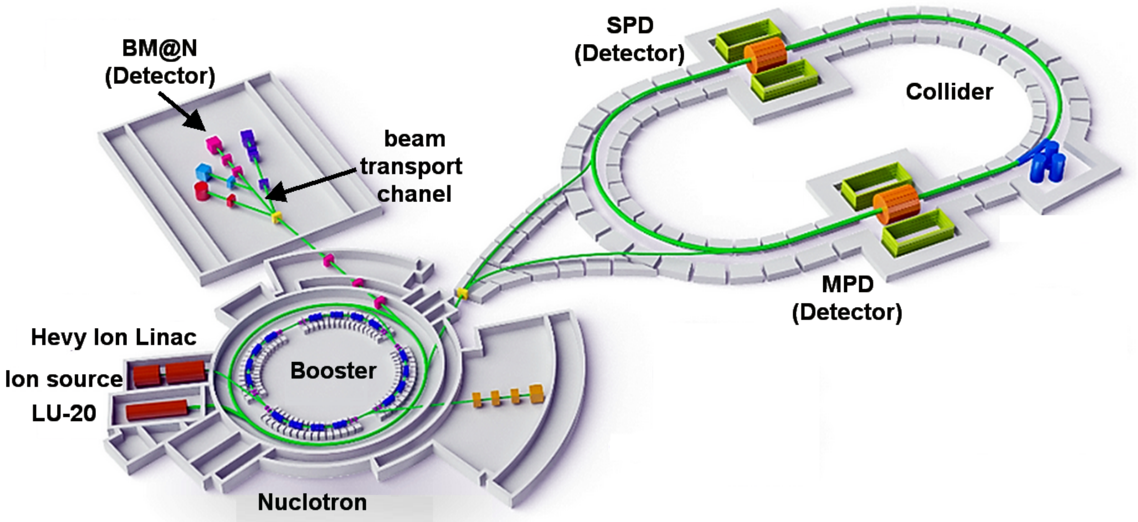

Figure 2: Complex NICA.

The beam extracted from the Nuclotron is transported to the BM@N experimental area over a distance of about 110 m by a set of dipole magnets and quadrupole lenses. At the entrance of the BM@N setup the position and direction of the beam are already close to those required to bring the beam to the target, and only relatively small adjustments are needed in order to provide final steering of the beam. These corrections are performed by a pair of dipole magnets, VKM and SP-57, which allow bending in vertical and horizontal planes and have maximum current 250A and 600A respectively. The centers of these magnets are positioned at approximately 7.7 and 5.7 m from the target (Fig. 3). In addition, a doublet of quadrupole lenses, 1k200 and 2k200, each having the maximum current of 2500A, allows optimal focusing of the beam on the target. The corresponding position of their centers is at about 12.5 and 10.0 m upstream of the target.

The target is located inside the analyzing magnet SP-41, therefore, after passing through the target, the beam ions are deflected by the magnetic field of SP-41 (maximum current 2000A, Bdl = xxx Tm). It should be noted that for experiments with heavy ions it is essential to enclose the beam transport channel in vacuum, including the part that goes through the analysing magnet. This requirement combined with precise placement of the tracking detectors inside the SP-41 does not allow quick reconfiguration of the detectors for different beam momenta, making it necessary to adjust the magnetic field of the analysing magnet depending on the choice of the beam momentum. Studies of the Xe + CsI collisions during the 2022-2023 run were performed at beam energies of 3.0 GeV/n and 3.8 GeV/n, and the current of the SP-41 was set to 1395 and 1720 A respectively.

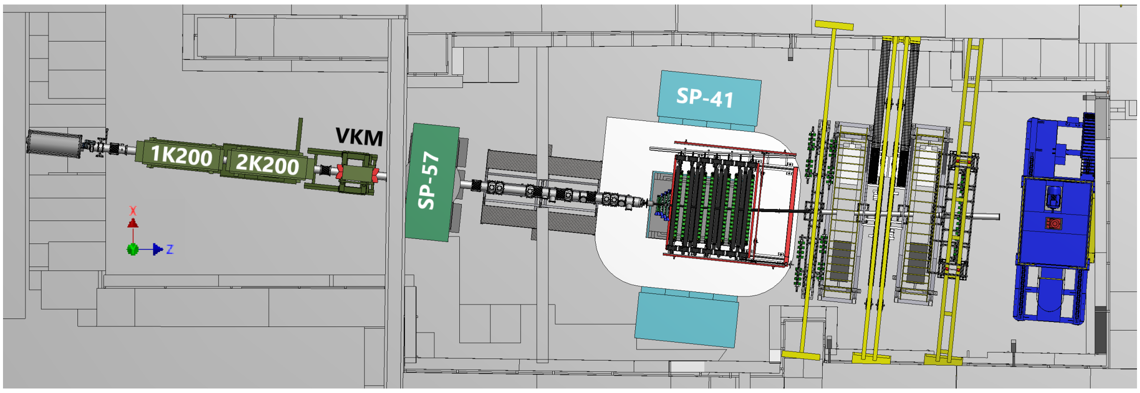

Figure 3: Magnetic elements of the BM@N setup.

2.2 Vacuum beam pipe

A vacuum beam pipe was integrated into the experimental setup in order to minimize the amount of scattering material on the way of heavy ion beam. The beam pipe has continuous vacuum, but in terms of components and material of the tube it can be subdivided into four large parts: the first section covers the region upstream of the magnet SP-57 and within the magnet itself, the second section goes up to the target, the third section is placed inside the analyzing magnet SP-41 and the last section is located after the analyzing magnet. Vacuum in the entire beam pipe at the BM@N setup is achieved by a single roots pump installed upstream of the 1K200 quadrupole lense. The pressure maintained during the experiment is at the level of 10^{-4} Torr. With the exception of the third part, the configuration of vacuum pipe and its components were designed, manufactured and tested by LLC Vacuum systems and technologies (Belgorod, Russia). ISO-K vacuum standard is accepted for flange connections, however, significant fraction of the components was custom made in order to meet limitations posed by aperture of the magnets and geometry of the detectors.

The first part of the beam pipe is designed to create vacuum in the area of beam transport through 1K200 and 2K200 quadrupole lenses and through corrective magnets VKM and SP-57. This part of the vacuum pipe is made of stainless steel, has length of 11.7 m and outer diameter 200mm. Two slide gates are installed in this section, one in the front of the 1K200 lense and another after the VKM magnet. The vacuum level is monitored by two vacuum gauges, the data from which are recorded in the slow control system.

The second part of the beam pipe serves to create vacuum in the region between the SP-57 magnet and the target node located inside the SP-41 magnet. This part of the beam pipe is xxx m long and also has outer diameter 200mm. It includes vacuum boxes containing beam detectors described in the next section: two 3-way boxes for profilometers, three 3-way boxes for silicon tracker and three 6-way boxes for trigger counters BC1, BC2 and VC. All boxes located outside the magnetic field of the analyzing magnet SP-41 are made of stainless steel, while the vacuum pipe components, which have to be close to the target and therefore placed in the magnet, are made of aluminum: compensator and three boxes for profilometer, Si beam tracker and BC2. Bending of the beam ion trajectories by the magnetic field leads to a deflection from a straight line resulting in a few mm displacement in X direction at the target location. During the assembly of vacuum elements of the beam pipe, an adjustment is carried out in order to compensate for this deflection. For that purpose the corresponding groves for O-rings of the vacuum boxes are made slightly wider than dictated by the ISO standard and allow slight off-center shifts of the vacuum pipe components. The target flange assembly is also made of aluminum as well as an ISO240 to 66 mm vacuum adapter for connection with the vacuum tube of the third section.

The third part of the beam pipe is 4.5 m long and made of carbon fiber by so-and-so producer. The entire carbon pipe consists of four straight segments of different lengths connected to each other by flangeless carbon fiber connections, which provide possibility to align sections at slight angles with respect to each other as shown in Fig. 4 and 5. The rotation angles were evaluated by the simulation of the 4.5 AGeV (???) gold ions trajectories in the magnetic field of SP-41 at current xxx A. The carbon beam pipe is suspended on two supports also made of carbon fiber and installed on two lower GEM detectors, the one closest to the target and the most downstream. The supports have adjustment units for precise positioning of the carbon beam pipe on the beam axis (Fig. 5). The carbon beam pipe was designed to sustain vacuum up to 10^{-4} Torr. In the straight segments the thickness is about 1 mm, while in flangeless connections it reaches 2 mm.

The fourth part of the beam pipe provides vacuum volume along the beam trajectory through

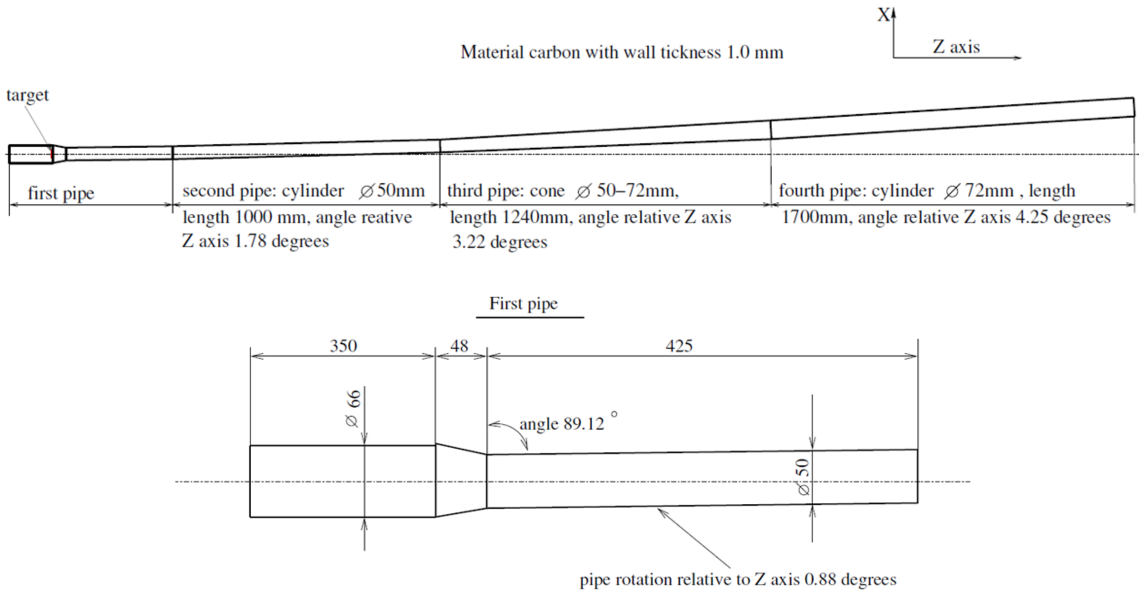

Figure 4: Technical design of the carbon beam pipe.

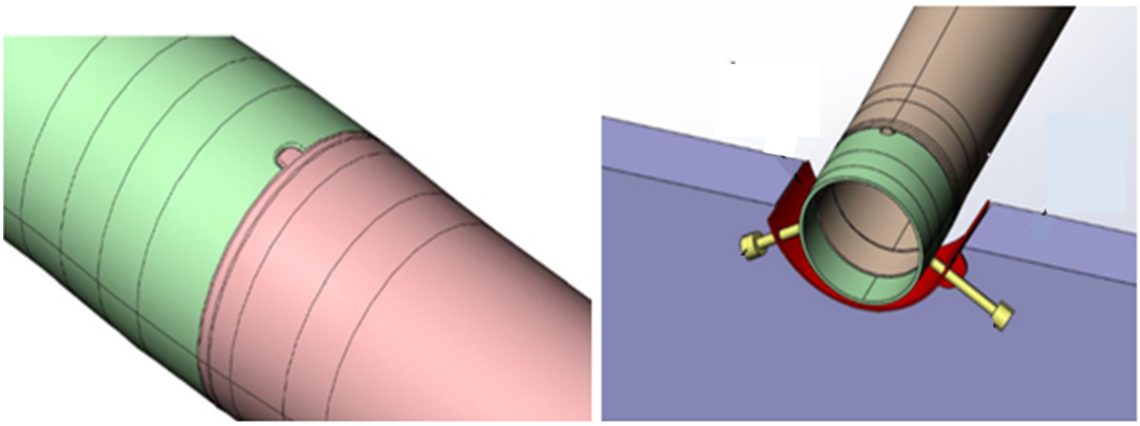

Figure 5: 3D models of the dismountable flangeless connection (left) and the support scheme of the carbon beam pipe in the GEM beam hole (right).

the outer tracker system. The pipes and flanges of this section as well as connection to the carbon beam pipe are made from aluminum (Fig. 6). It has overall length of about 3.2 m (?) and consists of three straight segments 1.2, 0.96 and 1.0 meter long, made from tube with outer diameter of 125 mm and wall thickness of xx mm. At the end of this section, the overall vacuum line is closed by a 100 μm thick titanium membrane installed in ... (?) after the adapter for a diameter of 150 mm.

2.3 Target station

The target station is located at the end of the second beam pipe section. It is designed to provide a possibility to insert a target in the beam line inside the vacuum volume and to interchange several targets without breaking the vacuum. The model and photo of the target station are presented in (Fig. 7). An aluminum flange of 240 mm in diameter serves as a holder of the target assembly elements and as an adapter between the beam pipe upstream of the target station and the first section of the carbon beam pipe. On the outer part of this flange, four pneumatic cylinders are installed providing capability to move in and out of the beam four target frames interchangeably. The pneumatic cylinders are produced by FESTO and allow remote operation. An optocoupler sensor is used in order to control the target position via a special electronic module.

The part of the target assembly placed inside the vacuum can be divided into three components:

1) Centering frame, which fits into the inner part of the first section of the carbon beam pipe.

2) Four petals, in which the targets themselves are installed. In the normal state, all petals are leaning against the side surface of the beam pipe.

Figure 6: Carbon beam pipe connected by a flange to aluminum beam pipe in the BM@N setup.

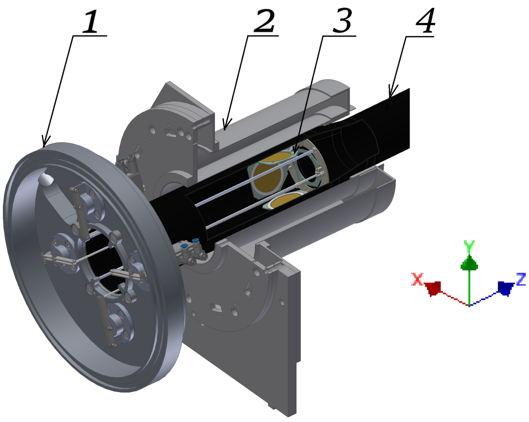

Figure 7: 3D model of target station. 1. Aluminum flange target station. 2. Barrel detector. 3. four targets. 4. Carbon beam pipe.

3) Carbon fiber retaining pins, 300mm long and 3mm in diameter.

In the run with the Xe beam, three disk targets about 3.2 cm in diameter were used: CsI 1.75mm thick, CsI 0.85 mm thick, and Ge 1.02mm thick. One frame of the target assembly was left empty and was used to evaluate the background level caused the particles interactions with the structural elements of the target station.

2.4 Magnetic field of the analysing magnet

The dipole magnet SP-41 with large acceptance is used in the spectrometer as analysing magnet for measurement of momenta of produced particles and beam fragments. In the course of preparation of the magnet for the BM@N experiment, significant upgrade was done in 2012-2013 from SP-41 initial configuration used in the experiments with a streamer chamber. In particular, the hole for a photocamera in the upper pole was filled with steel in order to improve the uniformity of the magnetic field, and the distance between the poles was increased by about 30 cm in order to provide space required by the GEM chambers of the BM@N. The dimensions of the SP-41 pole in the horizontal direction and in the direction along the beam is about 1.4 and 2.5 m, respectively, while the vertical distance between the upper and lower poles after the upgrade is 1.06 m (Fig. 8). In the BM@N setup the magnet is roughly centered on the beam line, in the horizontal plane the beam axis goes through the magnet close to the center of the poles, while vertically the beam axis is shifted closer to the lower pole by about 40 mm. The leading edge of the pole defines the origin of the z axis, and, correspondingly, the target is installed inside the SP-41 magnet at this position along the beam. The target station is described in more detail in the chapter Targets.

Determination of the momentum of the produced particles requires detailed knowledge of the value and orientation of the magnetic field of the analysing magnet. After the upgrade of the SP-41, the measurement of its field was performed by means of planar and 3D Hall probes [7]. In addition, the shape of the field was calculated by the TOSCA code using known configuration of the yoke and coils material. Prior to the run with Xe beam, in Spring 2022, the measurement of the magnetic field was repeated with a goal to obtain the field map for a wider X, Y, Z range and with smaller steps. The measurements with 3D Hall probes covered (-156, +145 cm), (-38, +54 cm), (-162, +439 cm) and were performed in (126 x 47 x 241) points in X, Y, Z coordinates respectively, allowing one to construct the field map on a 2.4 × 2.0 × 2.5 cm^3 three-dimensional grid (Fig. 8). During simulation and event reconstruction, the magnetic field components in a particular (x,y,z) point are calculated by linear interpolation over eight neighboring measured nodes.

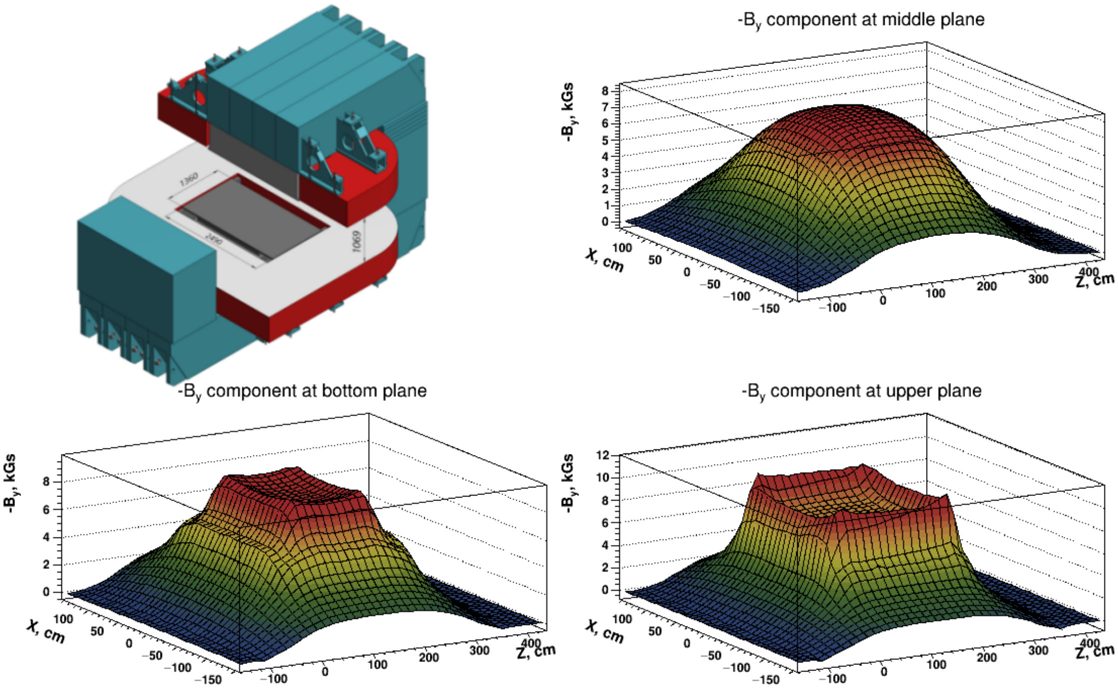

Figure 8: Magnetic field map of the analyzing magnet SP-41.

The measurements of the field map was performed for four values of the current: 900, 1300, 1600, and 1900 A.

Needed additions:

1) plot of field Vy versus current with points for 3.0 and 3.8 AGeV settings

2) explanation of "linear interpolation" for a 3D grid

3 Beam and trigger detectors

Fig. 9 shows a schematic layout of the trigger detectors, placed on the beam line. In the target area the multiplicity detectors are also shown as a part of the trigger system.

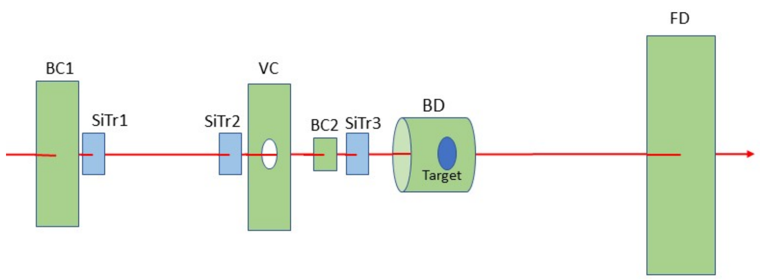

Figure 9: Trigger detectors layout.

Some physical parameters of the beam line detectors are summarized in Table 1.

Aperture of the beam is limited by the 25 mm diameter hole in the scintillation Veto Conter (VC), which rejects the beam halo. The hole diameter in VC is chosen to be large enough to accept most of the beam ions, but smaller than the diameter of the target XX mm. Typically, in the 2023 Xe run, 80% of the beam was accepted by the VC. In order to minimize interactions upstream of the target, scintillators and active parts of silicon detectors are located in vacuum, while the photomultiplier tubes of the scintillation counters and the front-end electronics of the silicon detectors are kept in the air with their housings mounted to the flanges of the beam pipe.

Detector	Z position, cm	Active area, mm x mm	Material	Thickness, mm
BC1	-zz	100 x 100	Scint. BC400B	0.25
BC2	-zz	34 x 34	Scint. BC400B	0.15
VC	-zz	113 x 113 (hole 25)	Plastic	4
SiBTr1	-zz	61 x 61	Silicon	0.175
SiBTr2	-zz	61 x 61	Silicon	0.175
SiBTr3	-zz	61 x 61	Silicon	0.175
FD	+zz	150 x 150	Plastic	0.5
Small GEM	+zz	100 x 100		
FQH	+zz	160 x 160	Quartz	4

Table 1: Parameters of beam and fragment detectors.

In all the beam scintillation counters - BC1, BC2 and VC - light from the scintillator is collected by Al-mylar light guides to a pair of photo-multiplier tubes, placed above and bellow the scintillator. Such orientation of PMT's in BC2 and VC detectors is dictated by the requirement that they should operate in the magnetic field of the analysing magnet, because these counters are located close to the target. Mesh dynode photomultiplier tubes Hamamatsu R2490-07 are used in the detectors BC1 and VC, whereas the BC2 has microchannel plate PMT's Photonis XPM85112/A1 Q400. In addition to beam geometry, the detectors BC1 and BC2 define start time for the time-of-flight system. The requirement to obtain precise time measurement favored the design of BC1 and BC2 with light collection by two PMT's. Both types of photo-multiplier tubes used in these counters have excellent timing characteristics. The signal from each PMT is sent to a fast fan-out module which has time jitter of about 10 ps and preserves high quality of time response. The signal from one output of the fan-out is sent to a TQDC which allows to determine time and amplitude of the pulse. After correction for time walk (slewing), the resolution obtained in 2022 Xe run using the signals from both photo-tubes was found to be 40 ps for BC1 and BC2 individually, and 30 ps for the combined response of the system of two counters. The input in the trigger logic is configured to accept one signal from each of the beam counters, BC1, BC2 and VC. Individual signals from top or bottom PMT's are affected by light collection non-uniformity to a larger degree than a combined signal from two photo-tubes. Therefore, in all counters the signals from top and bottom PMT's are balanced in gain by high-voltage settings, and the signals from the second output of the fan-outs are sent to a passive linear fan-in after which the summed signals are fed to the trigger logic unit. In addition, the summed signals are read-out using TQDC for trigger setting up and monitoring.

Upstream the target the beam position is traced by a set of silicon tracker detectors. The beam tracker system consists of three double-sided silicon strip detectors identical in design. Each detector has 60 mm by 60 mm active area with orthogonal orientation of p+ and n+ strips on two sides. These detectors are kept permanently in the beam and provide information about beam ion trajectory for each event. More detailed description of the beam tracker is given in the next chapter. In addition to the beam tracker, the beam position and profile can also be measured by a pair of beam profilometers which are similar in design and parameters to the beam tracker stations, but have a much courser pitch 1.8 mm in X and Y. The read-out of the profilometers is organised independently of the main BM@N DAQ in order to facilitate beam tuning at the early stages of the run. The detectors of the beam profilometers can be moved in and out of the beam by remotely controlled drivers without breaking the vacuum. During the data accumulation the detectors of the beam profilometers are positioned outside of the beamline.

Trigger detectors sensitive to the multiplicity of particles produced in the interaction include Barrel detector (BD) and Silicon multiplicity detector (SiMD). These detectors, schematically shown in Fig. 10, are placed close to the target in order to cover sufficiently large solid angle for produced particles. The target is situated inside the BD.

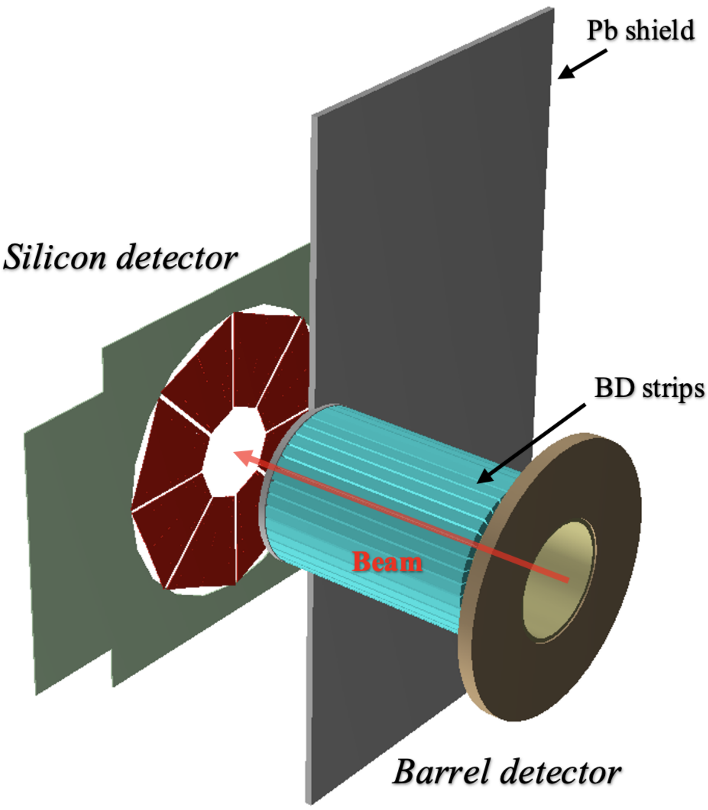

Figure 10: Schematic layout of trigger multiplicity detectors.

The Barrel detector is formed by 40 scintillator strips aligned along the beam line and covering cylindrical surface 90mm in diameter and 150mm long. Each strip of $150 \times 7 \times 7\,mm^3$ size is coated with aluminized mylar and viewed from one side by a silicon photo-multiplier of $6 \times 6\,mm^2$ size (SensL, J-ser.)

Downstream the analysing magnet the beam goes through the Fragment Detector (FD), Small GEM chamber and the Forward quartz hodoscope (FQH). These detectors are placed in the air, the FD is positioned right after the titanium membrane which closes the vacuum pipe line. The amplitude of the pulse in the FD reflects the charge of the ion passing through the counter. This amplitude is used in the trigger system in order to distinguish events with and without interactions in the target. To minimize the background from the interaction within the FD itself, its radiator has to be thin, while in the X and Y directions the radiator should be wide enough to cover all the beam ions going through the target without interaction. The radiator material can be chosen either from scintillator or quartz in experiments with relatively light (up to Xe) or heavy (Au, Bi) beams respectively. For most of data accumulation in the Xe 2022 run the scintillator radiator was used, while the quartz radiator was also evaluated in the short period of the run. The radiator was viewed by a single photo-multiplier tube placed about 50 cm below the beam line. Light collection is done by an air light guide made of aluminized mylar. Pulse height resolution of the FD with the scintillator radiator was found to be 5% for Xe peak.

In addition to the FD the charge of spectator fragment can be determined by the 4mm thick quartz hodoscope FHQ, located in front of the beam hole in the FHCal. Information from this hodoscope is used in the offline analysis for event selection and determination of event centrality. FHQ amplitude resolution for Xe ions is about 2%. The detailed description of the hodoscope is given in the section "Forward Spectator Detectors".

The Small GEM detector is positioned between the FD and FHQ and used to monitor the position, shape and spot size of the beam downstream the analysing magnet. The detector has three GEM foils. Its active area covers 10 cm$\times$10 cm in X and Y, with 256 strips in each coordinate oriented perpendicular to each other.

4 Silicon Beam Tracker

nzamiatin@mail.ru , yurij.kopylov.163@mail.ru

The Beam Tracker (SiBT) is located inside the vacuum beam pipe, directly in the beam of charged relativistic nuclei upstream of the target. BT consists of three coordinate planes (SiBT1, SiBT2, SiBT3) based on silicon double-sided strip detectors (DSSD). The main purpose of the beam tracker is the following physical tasks:

- measurement of the trajectory of xenon nuclei (124Xe) that pass through all three BT planes, the target (CsI) and satisfy the conditions of trigger logic;
- restoration in the target plane (X-Y) of the coordinates of the primary vertex of the trigger nucleus;
- information about the coordinates of the nucleus track in the area $BT1 \div BT3$ is involved in the reconstruction of the reaction plane;
- in the mode of beam adjustment and aiming the beam at the target, SiBT performs the function of a profilometer, the current information about the shape and position of the beam relative to the target is displayed on the monitors "On Line Monitor".

Each coordinate plane consists of one double-sided strip detector containing 128 strips on each side. Strips from different sides are arranged orthogonally and form a two - coordinate (X-Y) measuring system ($128p^+ \times 128n^+ = 16384 points$). The dimensions of the Si-crystal of the detector are $(63 \times 63 \times 0.175) mm^3$, the active area is $(61 \times 61) mm^2$, the strip pitch is 470 μm. The thickness of each DSSD silicon detector is 175 μm and is chosen as the minimum possible, taking into account the requirements of planar technology on silicon wafers of high-resistance silicon n-FZ-Si with a diameter of 4" (100 mm). The minimum allowable thickness of the detector was chosen based on the following considerations:

- the minimum amount of matter in the beam of heavy nuclei reduces the correlated background;
- the minimum volume of the active region of the detector (the region of the space charge of the detector) reduces the number of radiation defects per strip (less dark current, less noise in the registration channel);
- a large value of ionization losses $\Delta E = 245 MeV/175 \mu m/Si$ for Xe ($3.8 GeV/n$) allows one to effectively detect nuclei with a high signal-to-noise ratio ($S/N > 150$) in case of radiation damage to detectors.

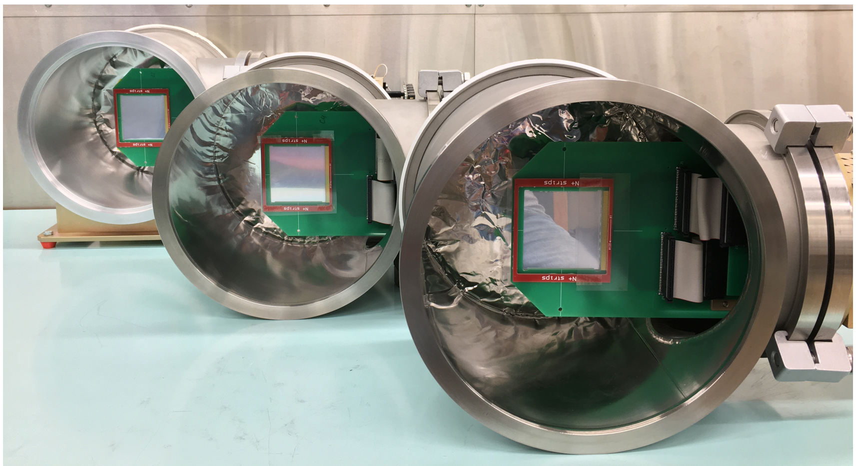

Figure 11: Three stations BT1, BT2, BT3 of the beam tracker of the BM@N experiment with detectors and FEE electronics, 256 channels, view along the beam (p^+ side of the strips).

Figure 15 shows three vacuum stations with internal coordinate planes based on silicon DSSD detectors installed inside. The positions of the coordinate system of the detectors of each plane relative to the geometrical axis of the beam pipe were measured using a NORGAU NVM II-5040D video meter with an accuracy of +/−50 µm. Structurally, the detectors are assembled on printed circuit boards with Au-contact pads, which are connected by ultrasonic bonding with Al-plated strips on the DSSD surface. The signals from the detector strips (256 strips) are sent via connectors on the board and flat cables to vacuum connectors (4 connectors) mounted on the vacuum flange. On the flange are placed 256 channel front-end-electronics (FEE) for 128p$^+$ strips and for 128n$^+$ strips. The detector electronics in this case is practically outside the zone of radiation damage and is available for testing and replacement of blocks without requiring depressurization of the beam pipe.

Figure 16 shows a block diagram of the integrated circuit VATA64HDR16.2 (IDEAS, Norway) with a large dynamic range ($-20pC \div +50pC$) for 64 channels of signal registration from detectors.

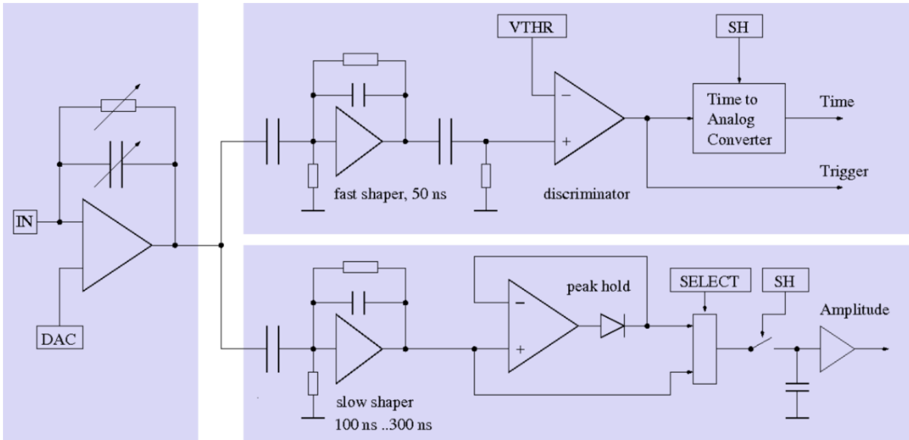

Figure 12: Block diagram of the VATA64HDR16.2 chip for the detector electronics of the beam tracker.

According to the signal "external trigger - SH", the values of signal amplitudes from 64 detector strips are stored on the memory capacitors and then in sequential reading mode through an analog multiplexer, the signals are transmitted to the ADC to convert analog signals into digital. The main parameters of the ASIC are given in Table 3.

Number of channels	64
Input charge (dynamic range)	-20pC ÷ +50pC (charge from 124Xe (3.8 AgeV) in 175 μm is 11 pC)
Read-out signal generation time	50ns, 100ns, 150ns, 300ns. Programming
Trigger	1 trigger output (Trigger-OR)
Trigger signal generation time	50ns
Noise	ENC = 1fC without load
Adjustable trigger threshold	External + 4-bit threshold trim-DAC/ch.
Gain	2-gain settings programmable
Exit	Analog multiplexed output 64 pulse height samples, serial output Differential current and voltage output
Power consumption per ASIC	960mW max. depending on settings
Nutrition	+2.5V, -2.5V

Table 2: Main parameters - VATA64HDR16.2

Figure 13 shows the dependence of the dark current of the Si detectors for three stations SiBT1, SiBT2, SiBT3 (three colors) on the exposure time to the beam of Xe nuclei (3.8 GeV/n). The fast component reflects the ionization current only in the presence of a beam, and the slow component (substrate under the fast one) integrates the accumulated radiation defects and reflects the constant (slowly increasing in time) dark current of the detector. The amount of radiation damage of the detectors corresponds to the number of Xe(3.8 GeV/n) ions passing through the detector planes, equal to $N_{Xe(3.8GeV/n)} = 4.44 \times 10^{10}$.

Figure **??** shows the working position of three stations of the beam tracker on the vacuum beam pipe of the BM@N channel. Each of the following SiBT stations following along the beam is rotated relative to the previous one by an angle of 30°. Rotation of stations relative to each other is done to

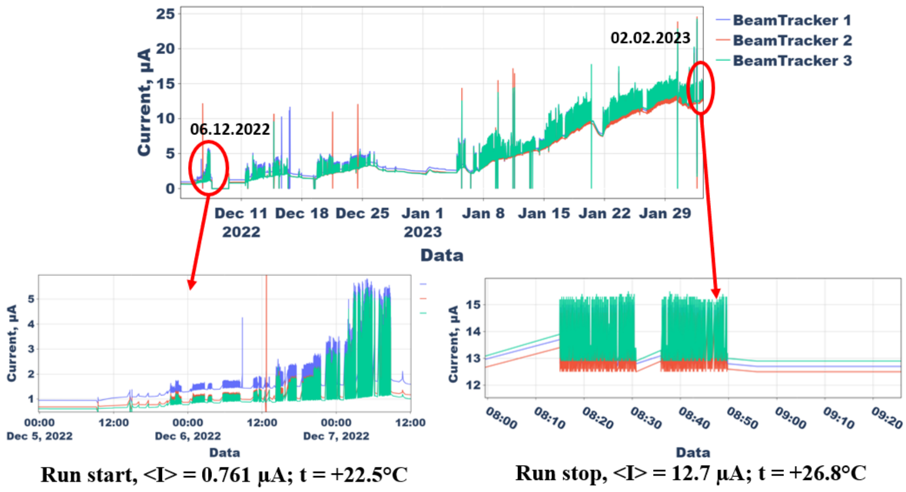

Figure 13: Chronicle of changes in the dark current of silicon detectors at stations SiBT1, SiBT2, SiBT3 in case of radiation damage during the session (from 06.12.2022 to 02.02.2023).

suppress false ("ghost") hits from simultaneous tracks, because the two-coordinate system in each plane (SiBT1÷SiBT3) is orthogonal. The arrows indicate the two-dimensional cross sections of the beam of Xe nuclei (3.8 GeV/n) measured by the corresponding stations SiBT1, SiBT2, SiBT3 and presented in the "On Line Monitor" mode.

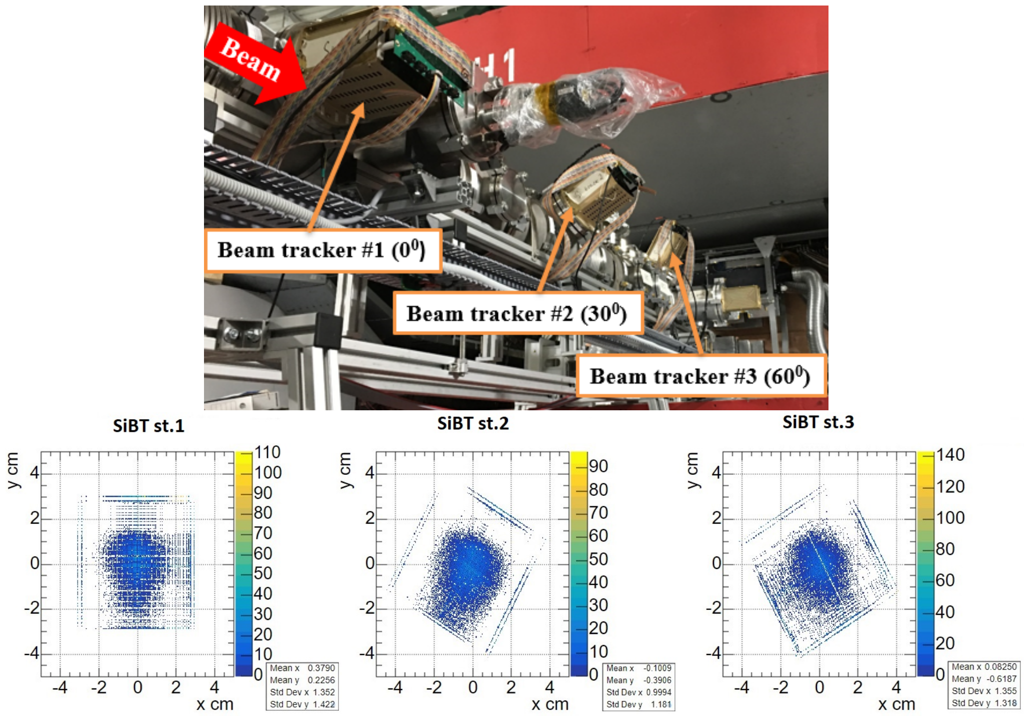

Figure 14: Operating position of three stations of the beam tracker on the vacuum beam pipe of the BM@N channel and two-dimensional beam profiles of Xe (3.8 GeV/n) nuclei measured by the corresponding BT stations.

The beam profiles shown in Figure 17 were obtained using the MBT trigger: counters BC1 and BC2 fired + VC not fired + FD not fired. The hole diameter VC is 25 mm, the average standard deviations of the X and Y coordinates for the profiles are 0.4878 cm and 0.5989 cm, respectively. The beam width can be estimated as 3 × Std(X) = 1.463 cm along the X axis and 3 ×S td(Y) = 1.797 cm along the Y axis.

5 Silicon Beam Tracker v2

As already mentioned in the previous section, the main task of the Silicon Beam Tracker (SiBT) is to measure the beam ion trajectory in each event and determine primary vertex coordinates and impact angle of the beam projectile. The tracker consists of three stations each of which utilizes a double-sided silicon strip detector (DSSD) with dimensions $(63 \times 63 \times 0.175) mm^3$. DSSD planes are cut from high-resistance mono-crystalline silicon obtained by the Float Zone method. The thickness 175 μm was chosen as the minimum possible, taking into account the limitations of the planar technology applied to 4" (100 mm) wafers. The minimum thickness of the planes allows not only to reduce the amount of material in the beam, but also to decrease the volume of space charge region of the detector and thus to lower the noise caused by the radiation defects per strip, which is very important considering that the detectors are exposed to heavy ion beams of high intensity.

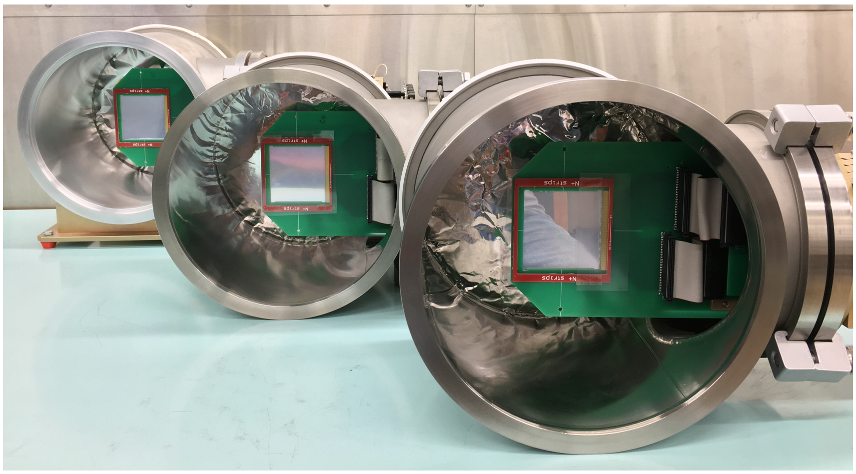

Figure 15: Three stations SiBT1, SiBT2, SiBT3 with detectors and FEE electronics, view along the beam (p^+ side of the strips).

The active area in each of the detectors is $(61 \times 61) mm^2$, and the pitch between strips is 470 μm on both, p+ and n+, sides resulting in total 2 x 128 readout channels. The strips on two sides are oriented orthogonally with respect to each other. The silicon plate in the SiBT1 detector is positioned inside the beam pipe such that the strips are aligned along the X and Y axes, whereas the plates of the SiBT2 and SiBT3 detectors are rotated azimuthally by 30 and 60 degrees respectively.

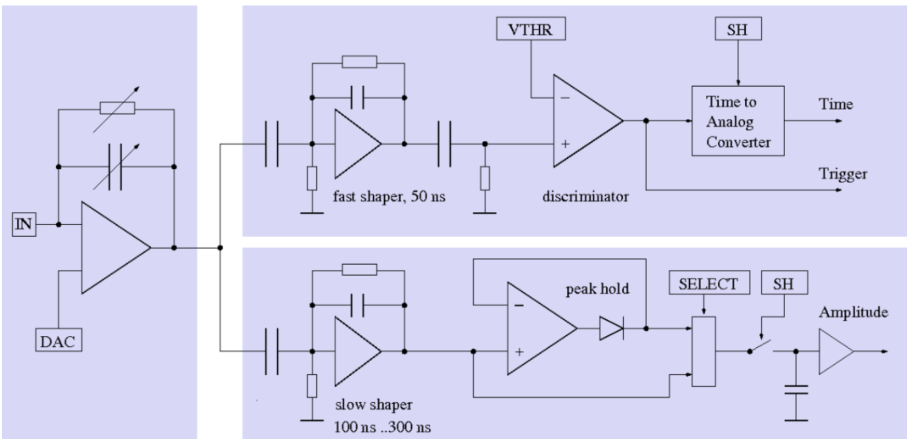

Figure 16: Block diagram of the VATA64HDR16.2 chip for the detector electronics of the beam tracker.

Figure 15 shows three vacuum stations with DSSD coordinate planes installed inside. The positions of the coordinate system of each DSSD plane relative to the geometrical axis of the beam pipe were measured using a NORGAU NVM II-5040D video meter with an accuracy of $+/-50$ µm. Structurally, the detectors are assembled on printed circuit boards with gold contact pads, which are connected by ultrasonic bonding with Al-plated strips on the DSSD surface. The signals from the detector strips in four groups of 64 channels are sent via flat cables to vacuum connectors (4 connectors) fixed in the vacuum flange. The front-end-electronics (FEE) for 128 p^+ and 128 n^+ strips is mounted on the flange outside the vacuum volume. The detector electronics in this case is practically outside of high radiation zone and is available for testing and, if needed, replacement without breaking the vacuum in the beam pipe.

Figure 16 shows a block diagram of the integrated circuit VATA64HDR16.2 (IDEAS, Norway), chosen for the FEE because of its large dynamic range ($-20pC \div +50pC$) suitable for operation with beams of highly ionizing heavy ions. For example, charge in the input signal caused by 3-4 GeV/nucleon Xe ion going through a 175 μm layer of silicon is 11 pC.

The ASIC VATA64HDR16.2 accepts up to 64 input channels, therefore, four of the chips are used in each of the SiBT stations. After passing through pulse shapers, at the time defined by "external trigger - SH", the values of signal amplitudes from 64 strips are stored on the memory capacitors. After that, in sequential reading mode using an analog multiplexer, the 64 signals are transmitted for digitization into a single ADC channel. The main parameters of the VATA64HDR16.2 chip are given in Table 3.

Number of channels	64
Input charge dynamic range	-20pC ÷ +50pC
Read-out signal generation time	50ns, 100ns, 150ns, 300ns, programmable
Trigger	1 trigger output (Trigger-OR)
Trigger signal generation time	50ns
Equivalent Noise Charge (ENC)	1fC without load
Adjustable trigger threshold	External + 4-bit threshold trim-DAC/ch.
Gain	2-gain settings, programmable
Output	Single analog multiplexed output of 64 pulse height samples
Power consumption per ASIC	960mW max. depending on settings
Voltage supply	+2.5V, -2.5V

Table 3: Main parameters of VATA64HDR16.2 chip.

Figure 17 illustrates three stations of the beam tracker mounted in the vacuum beam pipe of the BM@N channel. Histograms shown at the bottom part of the figure represent online monitoring of 2D distribution of beam ion hits in the tracker. Typical RMS of beam profile in the 2023 Xe run, measured for trigger selected events, i.e. for ions passing through the 2.5 cm dia. hole of the Veto Counter, was 0.5 cm and 0.6 cm in X and Y coordinates respectively.

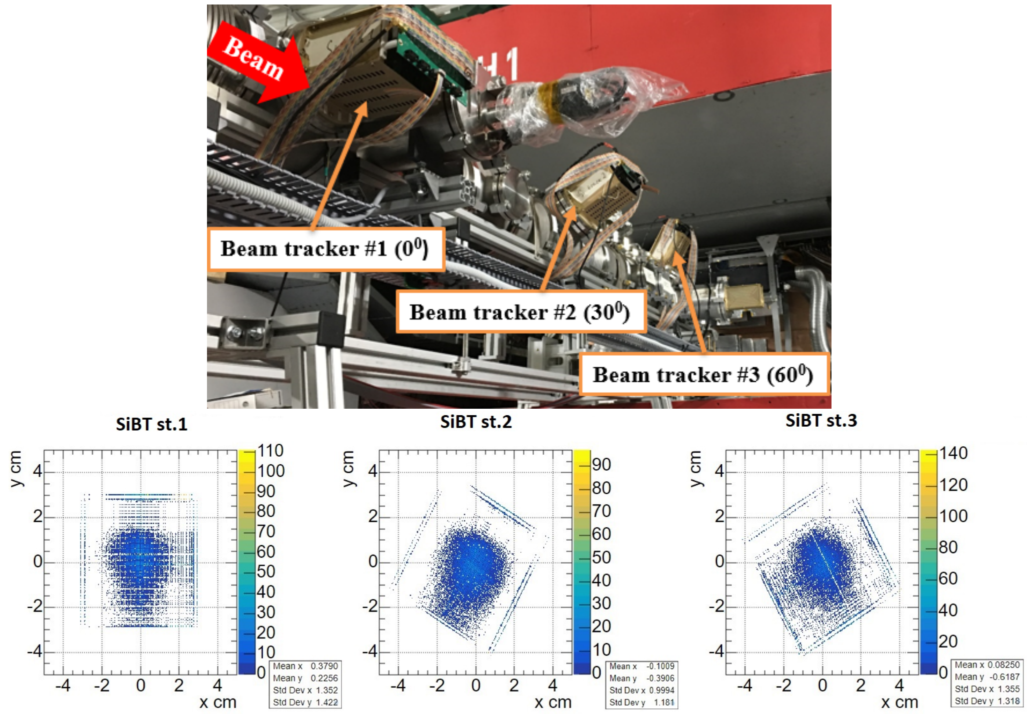

Figure 17: Operating position of three stations of the beam tracker on the vacuum beam pipe of the BM@N channel and two-dimensional beam profiles of Xe (3.8 GeV/n) nuclei measured by the corresponding BT stations.

6 Forward Silicon Detector

After the completion of the 2018 technical run at the BM@N facility, it was decided to develop and create a new four coordinate planes with an increased aperture in the front of the GEM chambers - Forward Silicon Detector (FSD). The new FSD design was supposed to increase the efficiency of particle detection and the accuracy of the primary vertex reconstruction for central interactions in the 2022–2023 run with the $_{124}$Xe beam (3.8 AGeV) interacting with the CsI target (2 % of nuclear interaction length). In addition to increasing the geometric dimensions of the planes, it became necessary to change the design of the planes due to the appearance of a beam vacuum tube on the BM@N channel. The presence of a section of a composite beam tube with a diameter of 50 mm after the target node required the division of the coordinate planes into upper and lower half-planes with the possibility of installing and removing detectors without touching the mounted and adjusted beam pipe.

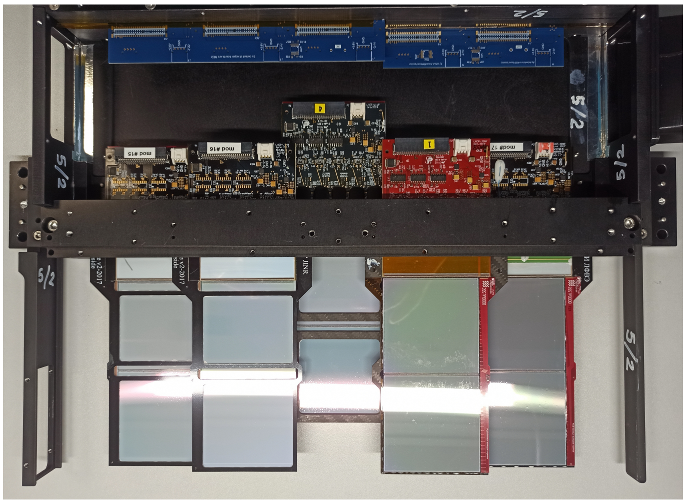

Figure 18: Appearance of the assembled 4 FSD planes (without cables) on the BM@N experiment channel inside the SP-41 analyzing magnet with the beam tube and target assembly installed.

The front part of the FSD central tracker (Fig. 23) is located in a vertical magnetic field of 1 T inside the analyzing magnet SP - 41 at a distance of Z_1 = 161 mm (first plane) and Z_4 = 466 mm (fourth plane) along the beam after the target. Each of the four silicon coordinate planes consists of two half-planes located perpendicular to the axis of the beam pipe. In the working position, the upper and lower half-planes form a single coordinate system of the plane with active regions overlapping along the Y-coordinate. In the center of each plane there is an insensitive zone in the form of a square with a cross section of 52×52 mm^2 to accommodate the beam tube. Each half-plane forms an independent coordinate detector with the following systems: coordinate modules based on DSSD, electronics backplane, suspension and precise positioning mechanics, cable patch panel, air cooling, temperature monitors, light and EM shield. The two half-planes of each plane are made structurally so that they are absolutely identical and interchangeable. This design allows the assembly or disassembly of the planes regardless of the installed beam pipe and with a minimum probability of its mechanical damage. The general view of the assembled eight half-planes around the beam tube inside the SP-41 magnet is shown in Fig. 23. The first plane consists of 6 modules of a new type, each module consists of one detector with dimensions of ($93\times63\times0.32$) mm^2, these are the maximum possible dimensions of a rectangular detector that fit on a Si-FZ wafer with a diameter of $\oslash$150 mm. Detectors of this type were developed jointly by ZNTC (Zelenograd) and LHEP JINR and manufactured at ZNTC in 2019–2020. The detector modules for the remaining three coordinate planes consist of two detectors with dimensions ($63\times63\times0.32$) mm^3, which were previously developed jointly RIMST and LHEP JINR and manufactured on n-FZ-Si wafers with a diameter of $\oslash$100 mm at RIMST (Zelenograd) in 2019 The total number of coordinate modules from which four planes are assembled is 48 pieces. Figure 19 shows the position and coordinates of the Si detectors relative to the target and the axis of the beam pipe. The aperture of the four planes in the direction of the Y coordinate is $\pm15°$ and in the direction of the X coordinate is $\pm30°$, which allows to cover completely the active area of the five GEM(#3 $\div$ #7) planes and the first GEM#1 planes along the beam, #7 FSD detector partially covers 50%.

Table 6 shows the quantitative data of the main functional elements of the coordinate planes that form the front part of the tracker (FSD). Coordinate planes with a spatial resolution better

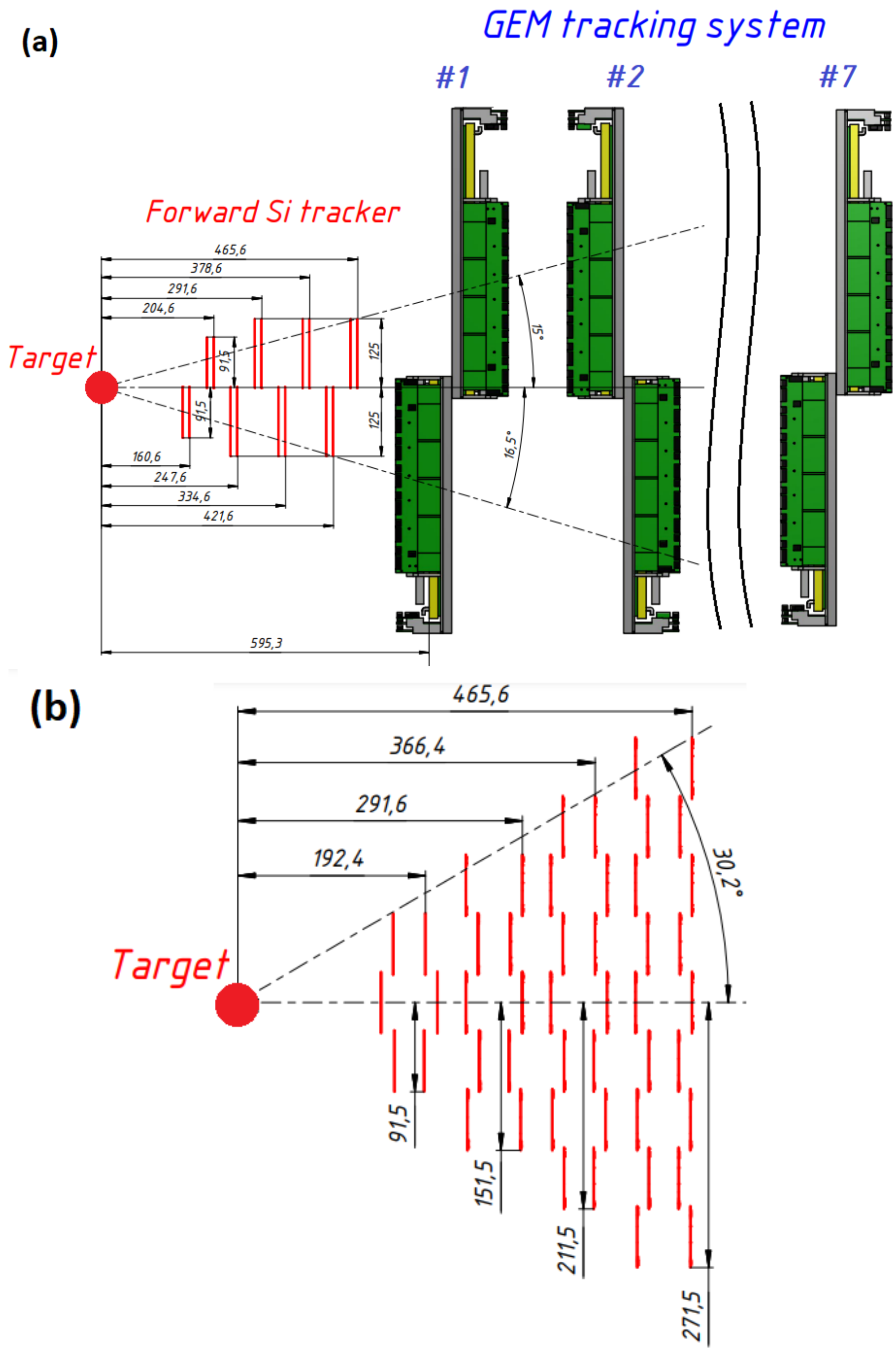

Figure 19: Scheme of the location of the FSD on the channel of the BM@N experiment (in the SP-41 magnet): (a) side view (YOZ), (b) top view (XOZ)

than 50 μm based on double-sided silicon detectors (DSSD) for detection of minimal ionization particles (m.i.p.) were first developed and created at JINR within the framework of the BM@N experiment. Figure 24 shows the external view of the coordinate module, which consists of two Si-detectors, two detector electronics (FEE) boards. This module has a sensitive detection area (186 $\times$ 63) mm ^{2}, 640 coordinate strips on each side and 1280 electronics channels (10 chips, 128 registration channels each).

The complete assembly process - testing of modules and planes is carried out on the production line for assembling LHEP modules. Double-sided silicon detectors (DSSD) and pitch adapters based on the SOS structure (Silicon on Sapphire) are manufactured at ZNTC (Zelenograd), until 2019, detectors were developed and manufactured at RIMST (Zelenograd) on high-resistance silicon wafers with a diameter of 100 mm (FZ-Si, n-type, ρ >5 k$\Omega\times$cm, <111>, ⌀100mm). The detectors have dimensions (63 $\times$ 63 $\times$ 0.3) mm^3 and contain 640 strips on both sides (p$^+$ and n$^+$), the strip spacing is 95 and 103 μm, respectively, and the angle between the strips is 2.5°. DSSD technology is

Parameters	1st plane	2nd plane	3rd plane	4th plane	Total
Number Si- modules	6	10	14	18	48
Number DSSDs	6 (93 × 63)mm^2	20 (63 × 63)mm^2	28 (63 × 63)mm^2	36 (63 × 63)mm^2	90
Number ASICs ($T \leq +25°$)	60	100	140	180	480
Dissipated power, W	16.86	28.16	39.42	50.69	135.13
Number PAs	12	20	28	36	96
Number FEE PCBs	12	20	28	36	96
Number of channels	7680	12800	17920	23040	53760
Square, m^2	0.035	0.073	0.102	0.132	0.307

Table 4: Main parameters of Forward Silicon Detector BM@N

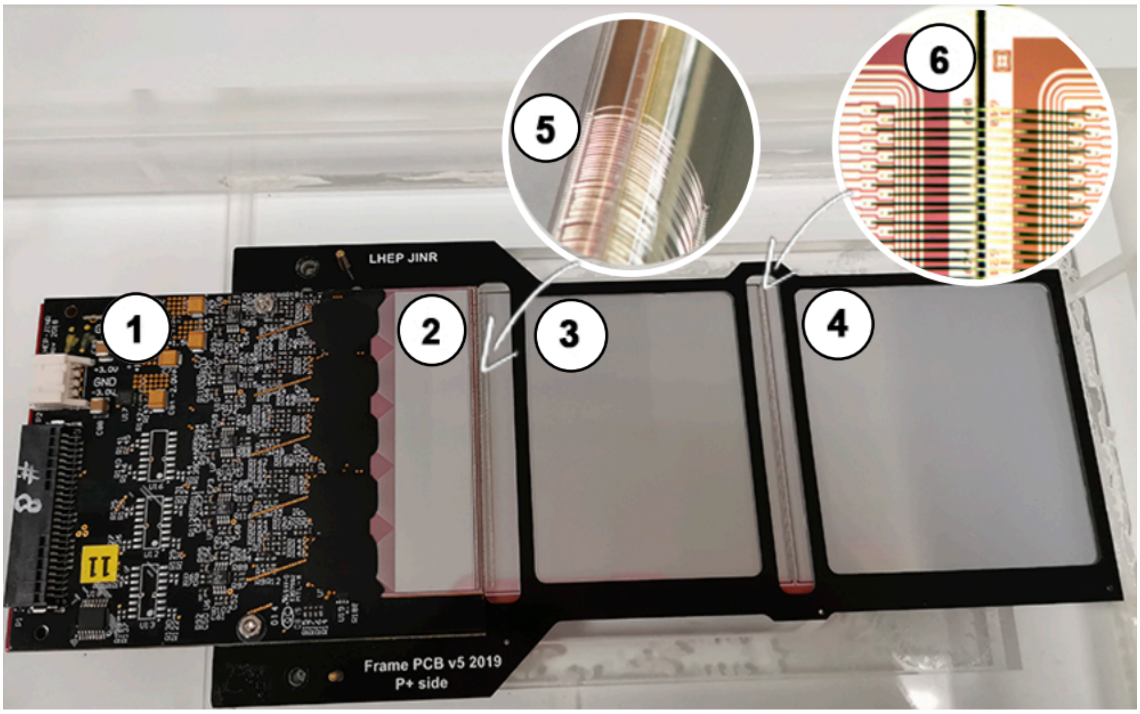

Figure 20: An example of a two-way US - bonding 2 - x DSSD on the FSD BM@N coordinate module

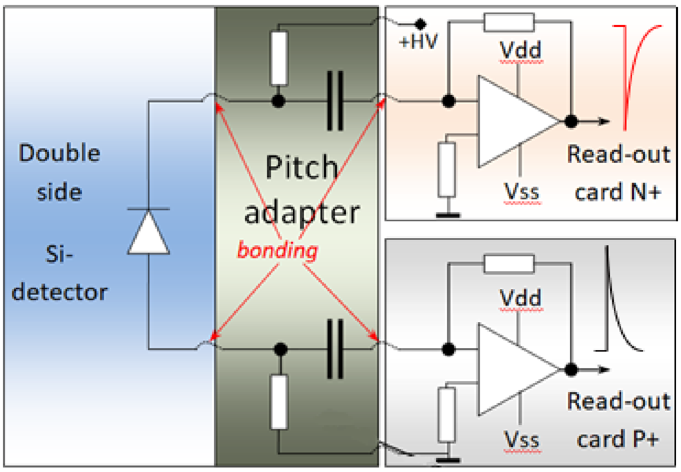

Figure 21: Functional diagram for reading signals from a silicon detector in a coordinate module

one of the most complex, because technological processes (growing thermal SiO_2, photolithography, ion implantation, annealing, metallization, etc.) are carried out separately on two sides of silicon wafers and usually with one detector placed on the wafer.

The module consists of two DSSDs with a sensitive area of (63 × 63) mm^2 each, mounted on a common frame with an accuracy of (± 20 μm), where the strips of the same name of one DSSD are connected to the strips of another DSSD by ultrasonic bonding (US-bonding) with an Al-wire ⊘ 25 μm . The detector topology (DC) does not contain integrated bias resistors and capacitors for DC decoupling of the strips from the inputs of the readout electronics. The role of the RC-bias element in the DC circuit is performed by the integrated Pitch-Adapter (PA), it also performs the matching of the strip pitch (pitch) with the topology of the pads of 128 inputs of the VATAGP7.2 chip. PA is made on the basis of SOS - structure (Silicon On Sapphire) contains integral capacitances and resistors. Each PA has 640 RC channels, polysilicon bias resistors are 1MΩ, and integral capacitors are 120pF/100V. PA-640 integrated circuits manufactured at ZNTC have low leakage currents (less than 10-12 A/capacitor/100 V) and an electrical breakdown value of 150 V, which corresponds to an electrical intensity in the capacitor of more than 3 MV/cm.

After PA, the signals from the p^+ and n^+ strips of the detector are fed to the inputs of a 128-channel specialized integrated circuit VATAGP7.1 (IDEAS, Norway). The value of the ionization loss signal (the maximum of the Landau-Vavilov distribution for 300 μm silicon) is 2.4×10^3 e (Q = 4 fK, or ΔE = 86 keV). Each electronic registration channel consists of: charging amplifier (σ - 200 e), shaper (t_s = 500 ns), memory capacitor and analog multiplexer 128 inputs to 1 output. On each printed circuit board, 5 microcircuits are mounted, welded into pitch adapters and sealed with a compound, which register negative polarity signals from 640 n^+ strips and positive polarity signals from 640 p^+ strips.

After assembling the half-planes, for each of them, measurements of the true position of the detectors were carried out using the NORGAU NVM II-5040D video meter with an accuracy of ±50 μm. The coordinates of the detectors and their rotation relative to the outer base points of the half-plane body were determined. Geodetic markers were subsequently installed on these base points, the measurement of the position of which in space made it possible to bind the position of each detector to the common coordinate system of the installation

Plane number	number of modules	number of channels	problem chips, pcs.	problematic channels, pcs.	problematic channels, %
#1 (3 × 2)	6	7680	0/0	0/ 0	0 / 0
#2 (5 × 2)	10	12800	0/1	0/ 128	0 / 1
#3 (7 × 2)	14	17920	0/1	0/ 128	0 /0.71
#4 (9 × 2)	18	23040	4/8	512/1024	2.2/4.4

Table 5: Number of problem channels of FSD registration before/after session No. 8 BM@N

Table 5 shows the data (see Fig. 26) based on the results of tests in space (before the run) and after the run on the 124Xe beam (3.8 GeV/n). Insensitivity on 128 channels=chip (dark bands in Fig. 14) may indicate the appearance of one of two defects:

- broken electrical contact in the transmission circuit from the chip (FEE buffer, cross-board connector, patch panel cable, long ADC-64 cable), this defect can be eliminated;
- failure of the chip (no programming of the operating mode), breakage of the US - bonding, this defect is unrecoverable.

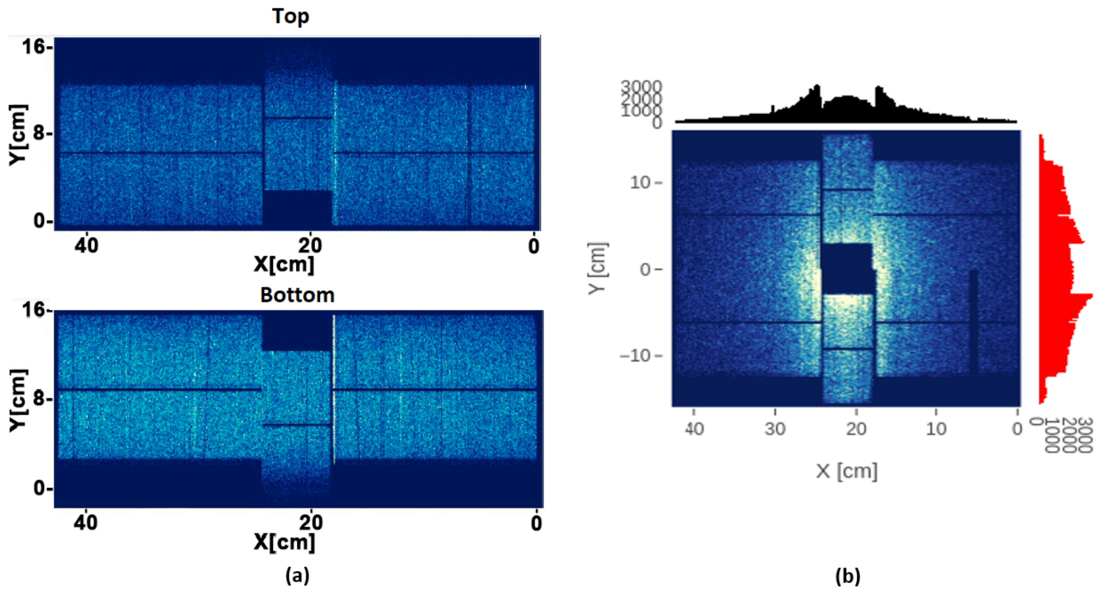

Figure 22: Comparative data on channel occupancy in space tests (a) and in Session BM@N (2022-2023) RUN # 7529 (11.01.2023), $t_c = 25.2°C$, Target #2 CsI (2%) (b).

7 Forward Silicon Detector v2

Two large tracking detector systems placed inside the analysing magnet are the Forward Silicon Detector (FSD) located right behind the target area, and a set of GEM detectors installed downstream, inside the interpole volume. FSD provides four tracking planes, while the GEM system consists of seven tracking planes. In order to accommodate the beam vacuum pipe going through the setup, each tracking plane in both systems is sub-divided in two half-plane detectors, upper and lower. This section describes the details of the FSD.

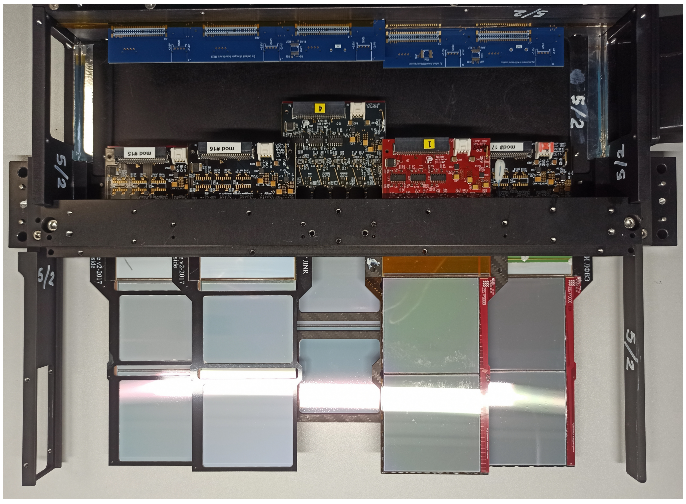

Figure 23: Appearance of the assembled 4 FSD planes (without cables) on the BM@N experiment channel inside the SP-41 analyzing magnet with the beam tube and target assembly installed.

Each half-plane of the FSD forms an independent coordinate detector with the following systems: coordinate modules based on DSSD, electronics backplane, suspension and precise positioning mechanics, cable patch panel, air cooling, temperature monitors, light and EM shield. Top and bottom halves of each plane are made structurally identical and interchangeable. In addition, the design allows vertical shift of the half-planes during the assembly in order to provide possibility to mount / dismount the planes regardless of the installed beam pipe and to minimize probability of its mechanical damage. In the working position, the upper and lower half-planes form a single coordinate system with active regions overlapping along the Y-coordinate. In the center of each plane there is an insensitive 52×52 mm^2 zone (larger ???) which makes room for the beam pipe. The general view of the assembled eight half-planes around the beam tube inside the SP-41 magnet is shown in Fig. 23.

The first plane consists of 6 modules each of which uses one DSSD with dimensions of (93 × 63 × 0.32) mm^2 positioned in such a way that the long side is aligned with the Y coordinate. The detector modules of the remaining three coordinate planes use two (63 × 63 × 0.32) mm^3 DSSD mounted on a common frame with an accuracy of (± 20 μm), where the strips of the same type of one DSSD are connected to the strips of another DSSD by ultrasonic bonding (US-bonding) with an Al-wire ⊘ 25 μm. Figure 19 shows the position and coordinates of the Si detectors relative to the target and the axis of the beam pipe, while Table 6 provides information about the number of modules and electronic components in each FSD plane.

The (63 × 63 × 0.32) mm^3 and (93 × 63 × 0.32) mm^3 DSSDs were manufactured at RIMST (Zelenograd, Russia) and ZNTC (Zelenograd, Russia) respectively. The detectors were cut from 10" and 15" high-resistance mono-crystalline silicon wafers produced by the Float Zone method (ρ >5 kΩ×cm). Each side, p$^+$ and n$^+$, contain 640 strips, the strip spacing is 95 and 103 μm, respectively, and the relative angle between the strips on two sides is 2.5°. The detectors are positioned in such a way that the strips of the p$^+$ side are aligned with the Y-axis.

Figure 24 shows the external view of the coordinate module with two DSSDs and a demonstration of US-bonding. The diagram of the signal input into FEE is presented in Figure 25. The detector topology (DC) does not contain integrated bias resistors and capacitors for DC decoupling of the strips from the inputs of the readout electronics. The role of the RC-bias element in the DC circuit is performed by the integrated Pitch-Adapter (PA), which also performs the matching of the strip pitch with the pad topology of inputs in the FEE ASIC. Manufactured also at ZNTC, the PAs were made on the basis of Silicon On Sapphire structure. Each PA has 640 RC channels with 1MΩ polysilicon bias resistors and 120pF/100V integral capacitors. The PA-640 integrated

Parameters	1st plane	2nd plane	3rd plane	4th plane	Total
Number of Si- modules	6	10	14	18	48
Number of DSSDs	6 (93 × 63)mm^2	20 (63 × 63)mm^2	28 (63 × 63)mm^2	36 (63 × 63)mm^2	90
Number of ASICs ($T \leq +25°$)	60	100	140	180	480
Dissipated power, W	16.86	28.16	39.42	50.69	135.13
Number of PAs	12	20	28	36	96
Number of FEE PCBs	12	20	28	36	96
Number of channels	7680	12800	17920	23040	53760
Area, m^2	0.035	0.073	0.102	0.132	0.307

Table 6: Main parameters of Forward Silicon Detector BM@N

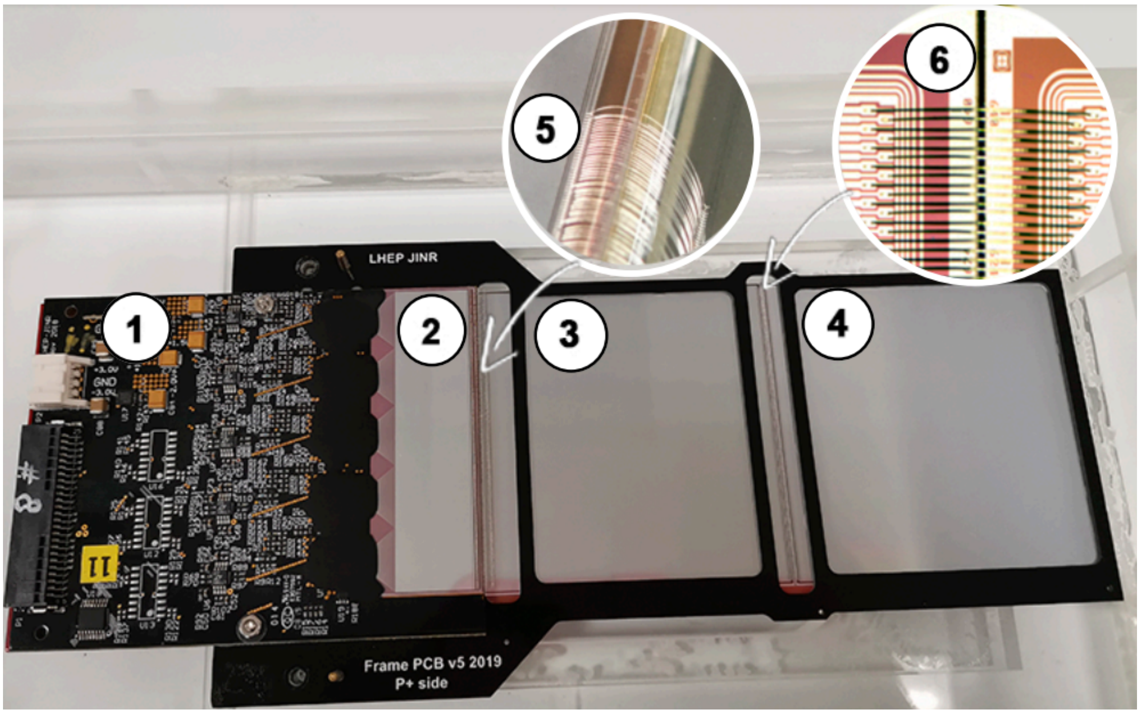

Figure 24: Example of two-way connection US – 2 – x DSSD on the FSD BM@N coordinate module: 1. Read-out electronics. 2. Peach Adapter. 3. DSSD1. 4. DSSD2. 5. Example of US - bonding PA + DSSD1. 6. Example of US - bonding DSSD1 + DSSD2.

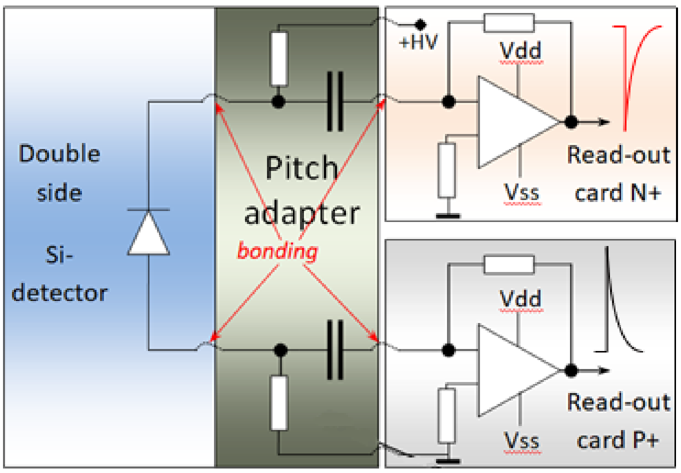

Figure 25: Functional diagram for reading signals from a silicon detector in a coordinate module

circuits have low leakage currents (less than 10-12 A/capacitor/100 V) and an electrical breakdown value of 150 V, which corresponds to electrical intensity in the capacitor of more than 3 MV/cm.

After passing the PA, the signals from the p^+ and n^+ strips of the detector are fed to the inputs of a 128-channel specialized integrated circuit VATAGP7.2 (IDEAS, Norway). (Is it VATAGP7.1 or VATAGP7.2 ???). Each electronic registration channel has a charging amplifier (σ - 200 e), a pulse shaper (peaking time t_s = 500 ns), and a memory capacitor which stores pulse amplitude at the trigger time. The ASIC also uses an analog multiplexer channeling 128 inputs to 1 output sent to the read-out in the DAQ by ADC. Two printed circuit bards are used in each FSD module in order to accommodate its input signals, one for 640 negative polarity signals from n^+ strips, the other for 640 positive polarity signals from p^+ strips. Correspondingly, 5 ASICs are mounted on each PCB, welded into the pitch adapters and sealed with a compound.

After the assembly of the modules in a half-plane, the position and rotation angles of every DSSD with respect to geodetic markers on the half-plane housing is measured using the NORGAU NVM II-5040D video meter with an accuracy of ± 50 μm. The markers are subsequently used during the installation in order to bind the position of each detector to the common coordinate system of the experimental setup.

Fig. 26 illustrates distribution of hits in the 4th plane of the FSD observed in the 2023 Xe run. Dark bands in the distribution indicate insensitive groups of 128 channels (1 chip). Number of such faulty chips at the end of the run was equal to 0, 1, 1, 8 for the 1st, 2nd, 3rd and 4th planes, respectively, which corresponds to 0, 1.0, 0.7 and 4.4 % of the channels. This malfunction can be due to the following reasons: 1) broken electrical contact in the transmission circuit from the chip (FEE buffer, cross-board connector, patch panel cable, long ADC-64 cable) 2) failure of the chip (no programming of the operating mode) or breakage of the US-bonding. Defects of the first type can be repaired, while the failings in the second group are of a permanent nature.

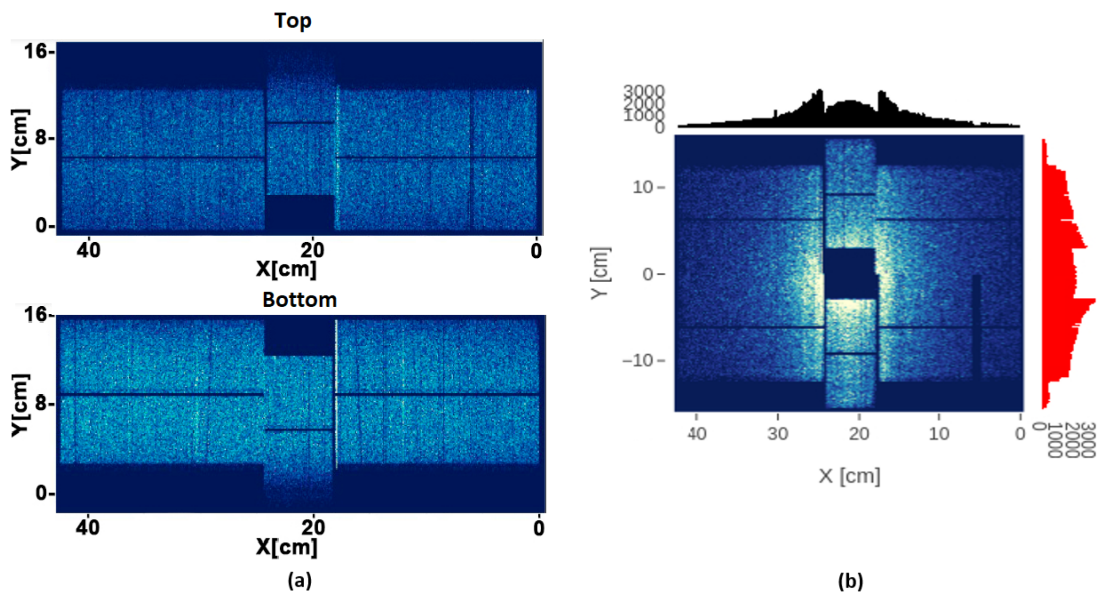

Figure 26: Comparative data on channel occupancy in space tests (a) and in Session BM@N (2022-2023) RUN # 7529 (11.01.2023), t_c = 25.2°C, Target #2 CsI (2%) (b).

8 GEM

Central tracking system is based on triple GEM detectors. Detectors are located inside the analysing magnet SP-41 downstream the FwdSi detectors. Due to the design features of the BM@N channel, in order to cover the maximum possible acceptance within the aperture size of the analysing magnet, the GEM detectors have been designed with two different active area sizes: 163×45 cm^2 and 163×39 cm^2.

Full configuration of the tracking system based on GEM detectors consists of 14 GEM detectors: 7 GEM detectors of the size 163×45 cm^2 – above the vacuum beam pipe (top GEM detectors), 7 GEM detectors of the size 163×39 cm^2 – below the vacuum beam pipe (bottom GEM detectors). The detectors form 7 planes through which the vacuum beam pipe passes. (Fig. 1)

BM@N GEM detectors were produced at CERN (PH Detector Technologies (DT) and Micro-Pattern Technologies (MPT) workshop).

8.1 Construction of GEM detectors

The GEM technology and the design of the BM@N GEM detectors are described in detail in [13]. Two different sector designs of BM@N GEM detectors are described in [14].

8.2 Front-end electronics

Front-end electronics are based on the charge sensitive preamplifier chip VA163 (IDEAS). A detailed description can be found in [15].

8.3 Mechanical support

For the precise installation of GEM detectors inside the SP-41 magnet, a mechanical support was developed. During development, it was necessary to take into account a number of parameters. All elements of the mechanical support must be made of non-magnetic material. The support frames that will be located next to the GEM detectors must be made of non-conductive material. Dimensions of GEM detector equipped with front-end electronics are 10 cm×182 cm×47 cm (bottom GEM detectors) and 10 cm×182 cm×52 cm (top GEM detectors) . The weight of one GEM detector equipped with mechanics, front-end electronics and cables is 19.5 kg. The detectors must be oriented strictly vertically. The whole assembly of 14 GEM detectors must be able to be vertically adjusted by ±10mm relative to the surface of the magnet coil. Each GEM detector must have a vertical alignment of ±5 mm with respect to the mechanical support. The installation accuracy of each detector relative to each other should not exceed 0.5 mm. It should be possible to move the whole assembly of 14 GEM detectors along the carbon beam pipe installed inside the SP-41 magnet without dismantling the detectors.

Mechanical support was designed and manufactured by LLC "Pelcom Dubna Machine-Building Plant".

Assembly of a mechanical support and installation of detectors on it consists of the following steps: 1) bottom detectors are installed sequentially, starting from the detector closest to the target; 2) a carbon beam pipe is installed on top of the bottom detectors; 3) top detectors are installed sequentially, starting from the detector closest to the target. Photo of installation process is shown in Fig. 27.

After each detector is installed, the front-end electronics are checked, a gas line is connected and detector is filled with gas mixture, high voltage is applied to the detector, and a radioactive source test is carried out. Then geodetic measurements of the position of the detector in a given coordinate system are made. At the same time, the detector goes through the adjustment procedure. The final results of the detector position measurements include coordinates of the corners of the detector and the center of the semi-circular notch for the beampipe. These values are necessary to correct the position of the detectors during the reconstruction.

The position and configuration of GEM detectors in Run 8 is shown in Fig. 28, Fig. 29.

8.3.1 Sequence of detectors in Run 8

To determine the sequence of GEM detectors in the magnet, the detectors were compared with each other. The number of unused channels and inefficient areas in the detectors were compared. Thus, the detectors that had regions of low efficiency in the side parts of the detector were installed closer to the target, where these regions are less significant for track reconstruction. Also, the top detectors with vertical sectors alternate with detectors with horizontal sectors.

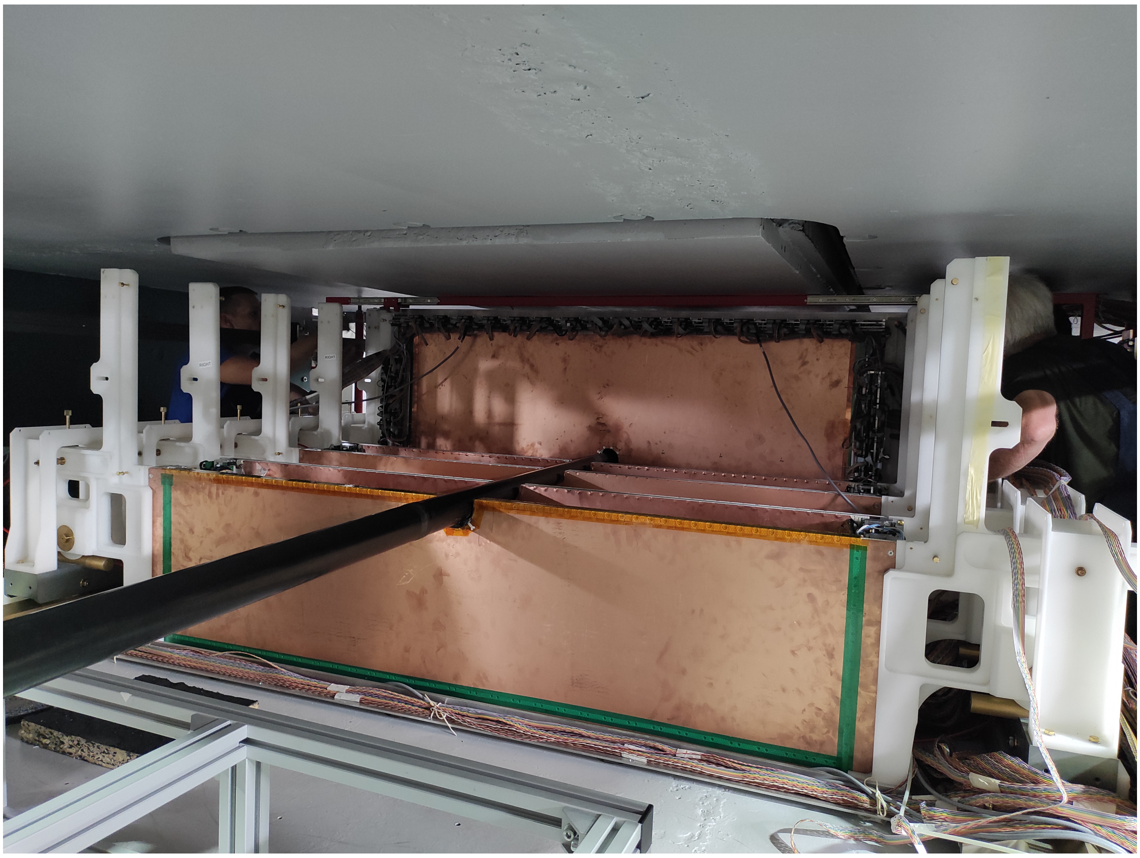

Figure 27: Photo of GEM detectors installation from back side of SP-41 magnet (in the direction opposite to the beam)

8.4 Gas system

GEM system was operated with gas mixture of Argon 80% and Isobutane (C_4H_{10}) 20%. The H_2O and O_2 removal filter was connected in line after the gas mixer. The gas line was divided into two identical lines for independent connection of the top and bottom GEM detectors. Two rotameters were installed on the lines, allowing to regulate the gas flow. Each line connected a group of top or bottom detectors in series, starting with the detector closest to the target. Small GEM detector was connected last in the line for the bottom detectors. The gas flow rate in each line was 3 l/h.

8.5 Small GEM detector

Small GEM detector was used to monitor the position, shape and spot size of the beam passed through the target and tracking system inside the analysing magnet. At the beginning of the Run 8, it was installed downstream the SP-41 magnet. And then, after adjusting the beam, it was moved behind a large CSC, so as not to interfere with the installation of an aluminum beam pipe downstream the SP-41 magnet. Small GEM detector is also consists of three GEM foils. The size of the active area is 10 cm×10 cm. The readout has two coordinates and contains a set of perpendicular strips of width ??. Number of channels of each coordinate is 256.

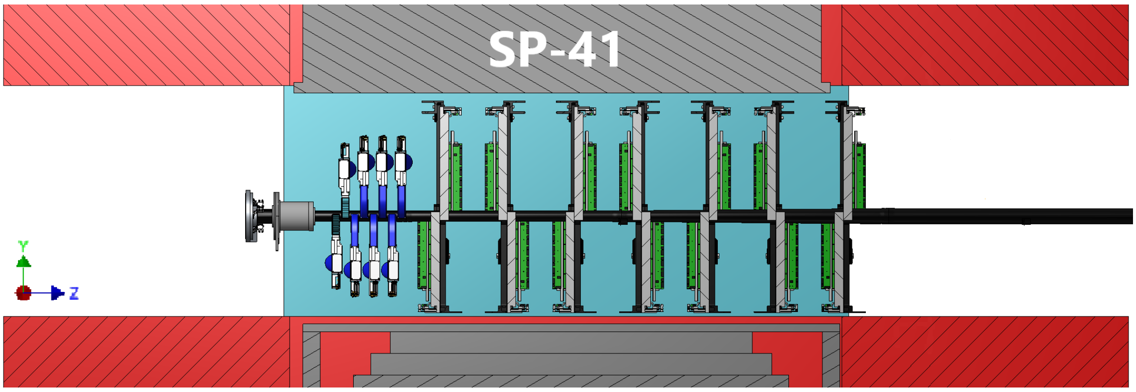

Figure 28: The position of GEM detector package relative to the magnet coil

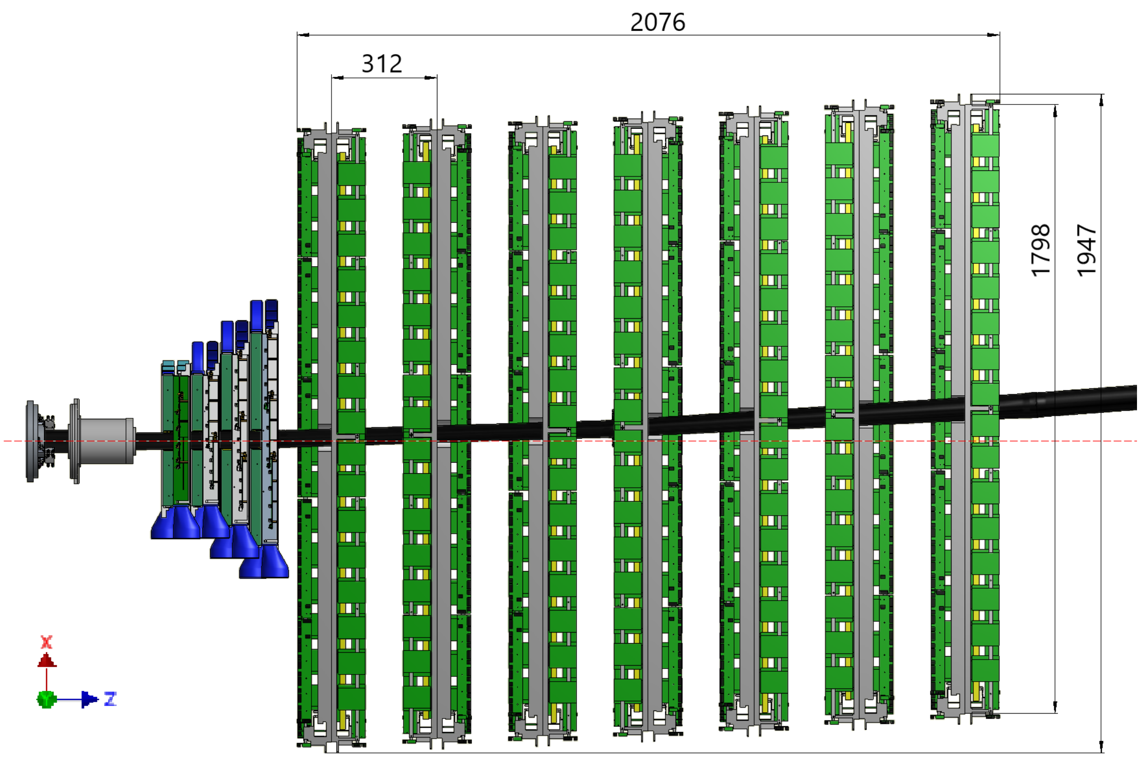

Figure 29: Displacement of detectors relative to each other due to beam pipe bending

5

9 TOF

(*RumyantsevM.mikhail.rumyantsev@yandex.ru*)

For charge particle identification the two Time-of-flight systems are used in BM@N. The first TOF system is placed at about 4 meters from the target and looks like two arms to the left and right of beam axis (TOF-400). The second TOF wall (TOF-700) is located at a distance of 7 meters from the target (fig 1). The arrangement of both systems provides continuous geometric acceptance and overlap with the external track systems. The basic requirements to the TOF system are:

- high granularity to keep the overall system occupancy below 15% and minimize efficiency degradation due to double hits;
- good position resolution to provide effective matching of TOF hits with tracks;
- high combined geometrical and detection efficiency (better than 85%);
- identification of pions and kaons with $0.1 < p_t < 3$ GeV/c;
- identification of (anti)protons with $0.3 < p_t < 5$ GeV/c

To achieve these goals, a strip-readable Multigap Resistive Plate Chamber (MRPC) detector was chosen for both TOF systems. This type of detectors is widely used for time-of-flight measurements (ref....). It showed good efficiency, high time resolution, the ability to work with particles flux up to tens kHz/cm^2.

9.1 TOF400

The TOF400 system consists of two part ~~are~~ placed left and right to the beam. Every part consist of two gas boxes (modules) with 5 MRPCs each (fig...). The active area of the MRPCs overlap on 50 mm inside the box. Gas box made from aluminum frame covered by aluminum honeycomb for reduction of radiation length. Overlap of gas boxes ensures crossing of active area of detectors 50 mm also. Active area of every part is 1.10x1.3 m^2 and defined to satisfy the geometrical acceptance of the GEM tracking detectors. The main parameters of the TOF400 are present in Table 7.

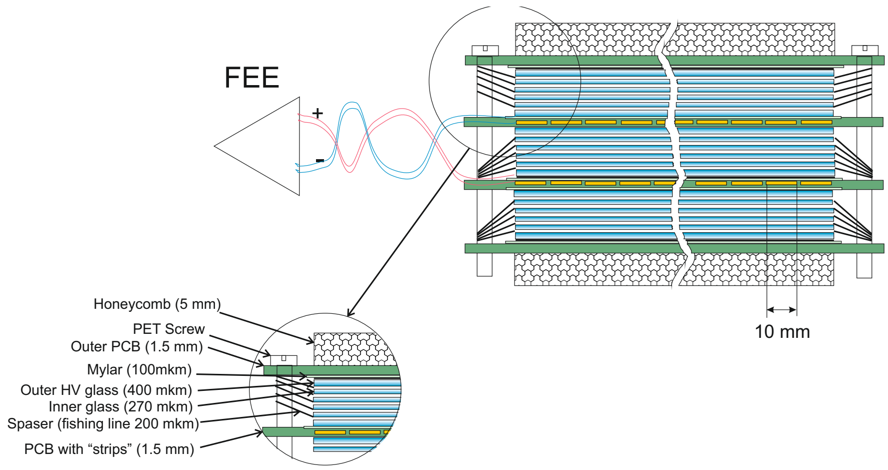

Figure 30: Schematic view of the MRPC detector for TOF400 system

A scheme of MRPC for TOF400 system is shown on Fig. 30. The detector consists of three stacks of 5 gas gaps each. Float glass with a thickness of 420 μm for external electrodes of the stack and 240 μm for internal ones was used as resistive electrodes. The fishing line as a spacer defines the 200 μm gap between all resistive electrodes. The outer part of external glass electrodes is covered by conductive paint with surface resistivity about 2-10 M$\Omega/\square$ to apply high voltage. All internal glasses are floating. The pickup electrodes look like strips and made on the PCB board. The main feature of the proposed triple-stack MRPC is that readout strips are located only in the inner stack. This ensures that the construction is symmetric, and speed of signals on the anode and cathode are the same, what prevent the dispersion of the signal. Differential analog signal from strip is transferred by twisted pair cable to front-end electronics. Signal is reading out from both ends of the strip. It provides better time resolution and determination of the coordinate of a particle along the strip. For stiffening structure we glue paper honeycomb with a thickness of 10 mm on outer part of the external PCBs. Dimension of active area of one MRPC is 300*600 mm^2. It has 48 readout strips, 10 mm wide and 300 mm long. To reduce crosstalk the gap between strips is 2.5 mm. Thus the pitch of electrodes in this case is 12.5 mm.

The charge sensitive NINO chip was used for TOF400 []. The chip has 8 channels and processed on 0.25 μm technology. Each channel includes ultra-fast preamplifier with a peaking time less than 1 ns, discriminator with a minimum detection threshold of 10 fC and output stage which provides LVDS output signal. The duration of the LVDS signal is proportional to the charge of the input signal, so it can be used for so-called amplitude-time correction. The 24-channel amplifier-discriminator base on NINO chip was developed in LHEP JINR []. Measurements with a test signal from the generator showed an intrinsic time resolution of the amplifier of 7 ps. The amplifier are placed as close to the MRPC as possible on front cover of the gas box. The signal from the preamplifier can be transmitted over a distance of up to 10 m via a special cable without loss of time resolution. Additional features of the FEE are the ability to remotely control the threshold, measure the supply voltage and temperature on the board via the RS485 interface.

72-channel time-to-digital converters (TDC72VHL []) based on HPTDC chip [] were developed in LHEP JINR for digitization of LVDS signals and data acquisition. The TDC72VHL operates in ultra high resolution mode with a bining of 23.4 ps. This allows to measure the leading and trailing edges of the input LVDS signal with high accuracy, but there is significant integral non-linearity at the TDC. This nonlinearity causes strong degradation of time resolution. The method of uniform filling the time gap with random events (code density test) was used for calibration (consideration of nonlinearity) of TDC module. The intrinsic time resolution of an individual TDC72VHL channel averaged 20 ps after applying the calibrations.

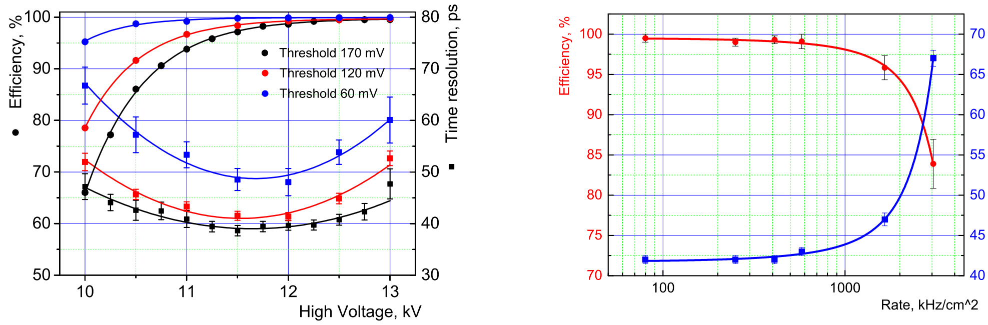

(a) (b)

Figure 31: Performance of the MRPC designed for TOF400 system. The detector efficiency and time resolution as function of applied of HV for different NINO thresholds are shown on the left. The right shows the dependence of the detector performance on the particle flux for 11.5 kV and 120 mv threshold.

The prototype of full scale MRPC with full readout chain was tested on the Nuclotron beam at LHEP. The deuteron beam was transferred to the experimental setup “Test MPD” []. The fast Cherencove counter [] with time resolution of 37 ps was used as a start detector. The result of measuring the efficiency and time resolution are present on the Fig. 31a . All results include contributions from the front end and data acquisition electronics. The efficiency is higher than 98% and time resolution is below 50 ps for different threshold of NINO. A voltage of 11.5 kV and a threshold of 120 mV were chosen as the operating point. Results of high rate test are presented on Fig. 31b. MC simulations show that the particle flux on the TOF400 does not exceed 1 kHz/cm2, so a time resolution of less than 50 ps and an efficiency of more than 95% are expected.

9.2 TOF700

The TOF700 wall placed at about 7 meters from the target and made of MRPC of different size in an individual gas box each. The wall size of 3.2x2.2 m^2 is defined to satisfy the geometrical acceptance of the outer tracking detectors (DCH). The detectors are mounted on two subwalls in two layers on each to provide a geometric overlap between the detectors. Both sub walls can move relative to each other to provide access for installation and maintenance. Two types of detectors are used for TOF700: a "cold" MRPC with an active area of 30.3x56 cm^2 (16 strips of 18x560 mm^2) for the area with a low particle flux and a "warm" MRPC with an active area of 16x35.1 cm^2 (32 strips 10x160 mm^2) for the area near the beam line. The main parameters of the TOF700 are present in Table 7.

A schematic cross-section of a "cold" MRPC is shown in Fig. 32. It consists of two identical stacks with five gaps each. Each stack is formed by six glass plates 0.67 mm thick with the bulk resistivity of 2x10^{1}2 $\Omega\times$cm. The gap between the glasses 0.3 mm is fixed by spacers (fishing-lines). Graphite conductive coating with surface resistivity of 1 $M\Omega/\square$ is painted to outer surfaces of external glass plates to distribute both the high voltage and its ground. The anode readout plate is a 100 $/mu$m one-sided printed PCB and is placed between stacks. Unipolar signals are taken from both ends of the reading strips, which makes it possible to determine the coordinate of the particle along the strip. Each detector is placed in an individual gas box. The bottom cover is made of PCB 2.5 mm thick and is designed to take out a signal from the box volume to readout electronics. The frame of the box is made of aluminum 2.5 mm thick. The top cover is made of 1.5 mm thick aluminum sheet. The box covers are reference plan for a unipolar signal. Warm MRPC is built in the same way as cold mRPC. However to increase the ate capability the gas gaps and the thickness of the glass plates are reduced (0.22 mm and 0.55 mm respectively). To compensate for the loss of the signal amplitude due to the increasing of the anode strip-cathode capacity, the number of gaps in the chamber was increased from 10 to 12 (six gaps per stack).

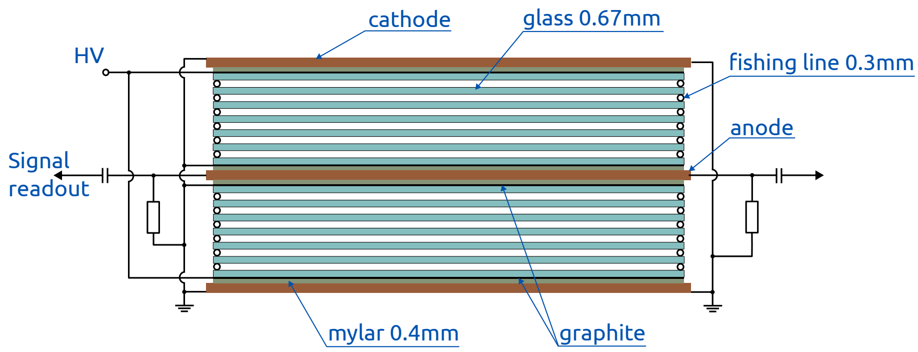

Figure 32: Schematic view of the MRPC detector for TOF700 system

The AddOn board base on NINO chip developed for the HADES experiment was chosen as front-end electronics (FEE) for TOF700. Signals from the MRPC to the FEE (32RPC) are received over 50 ohm coaxial cables using MMCX connectors. The LVDS output signals are transmitted to the digitizing module using DHR-78F connectors. A 64-channel VME TDC64VHLE time-to-digital converter based on the HPTDC chip is used for digitization. With a special module (PWR&CTRL) it is possible to remotely control the power supply, the discrimination threshold and hysteresis value on the FEE.

Prototypes of "cold" and "warm" detectors were tested on the secondary muon beam of the U-70 accelerator at IHEP. The test was carried out on the "MUON" facility with a particle flux of about 1 kHz/cm^2. A fast scintillation counter with its own time resolution of 40 ps was used as T0. The test results of both prototypes are shown in the figure 33. The intrinsic time resolution of the MRPCs with electronics is better than 45 ps with an efficiency of 98% and 95% for "cold" and "warm" chambers respectively.

9.3 Services system

Both TOF400 and TOF700 systems use the same a non-flammable Freon rich gas mixture containing 90% C2H2F4 + 5% i-C4H10 + 5% SF6. A simple open-loop gas system was designed for the BMN experiment. This system is based on the MKS 1479A controllers for measuring and adjusting the absolute flow of components with an accuracy of 0.3%. The flow rate of the gas mixture can be adjusted in the range from 6 l/h to 90 l/h, but the typical value is 21 l/h, which corresponds to the exchange of 2 volumes per day. Also, one additional channel is available for purging the system with nitrogen for cleaning and drying. A special PC program has been written to control the parameters of the gas system via the Ethernet interface.

The MRPC detector operates at very high voltage of 12 kV and 15 kV for TOF400 and TOF700 respectively. On the other hand, the dark currents of the detector are quite small at the level of

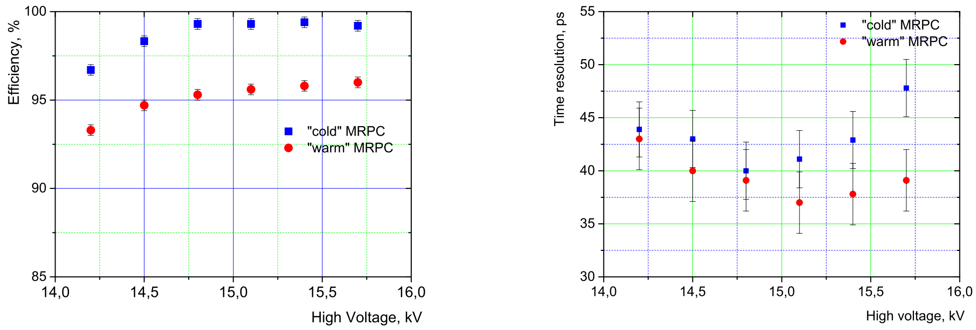

(a) (b)

Figure 33: Performance of the MRPC designed for TOF700 system. The detectors efficiency are shown on the left and time resolution are shown on the right.

	TOF400	TOF700
MRPC active area	30x60 cm^2	30.3x56 cm^2 "cold" 16x35.1 cm^2 "warm"
FEE on one MRPC	96	32 for "cold" 64 for "warm"
Number of MRPC	20	30 "cold" 40 "warm"
Total active area	2 Arms x 1.1x1.3 m^2	3.2x2.2 m^2
Total number of FEE	1920	3520

Table 7: Main parameters of TOF system.

tens of nA. Also, the detector is very sensitive to voltage ripples due to the large capacitive coupling between the high-voltage layer and the readout strips. Therefore, the high-voltage system is subject to high requirements for voltage stability and current measurement accuracy. The high-voltage power supply systems for both TOF are based on commercially available ISeg modules and a specially designed HVSys power supply. All elements of the system have the ability to remotely control via Ethernet interface.

To monitor of stability of operation of the TOF systems all controlled parameters are sent to the Slow Control System. The data is displayed on the website of the experiment via Grafana. The operator can see the value of the high voltage and current on the detectors, the set voltages and thresholds of the amplifiers, the gas flow and the weight of the gas in cylinders, and other parameters. In case of an emergency, the operator receives a message that allows to respond in time. All data is stored in a database and can be used for further analysis.

10 Outer tracker

The purpose of the outer tracker is to provide link between tracks measured in the central tracker and hits in the ToF-400 and ToF-700 detectors. In the Run 8 outer tracker consisted of two large aperture drift chambers (DCH), four CSC (cathode strip chamber) with the size of the active area of 1129×1065 mm^2 and one plane of 2190×1453 mm^2 CSC (see Fig. 1).

10.1 DCH

The drift chambers [16] have an octagonal shape with a transverse width of 2.9 m. (Fig. 34).

Figure 34: DCH integrated into BM@N experimental setup.

Their fiducial area is about 4.5 m^2. Every drift chamber (DCH) consists of 4 double coordinate planes with the following parameters: the wire inclination angles of 0^o, 90^o, $\pm 45^o$, the wire pitch of 10 mm, the outer dimentions of the sensitive area of Yout ± 1.2 m, Xout ± 1.2 m, the beam hole radius of R = 160 mm, 256 wires per coordinate plane, 2048 wires per chamber.

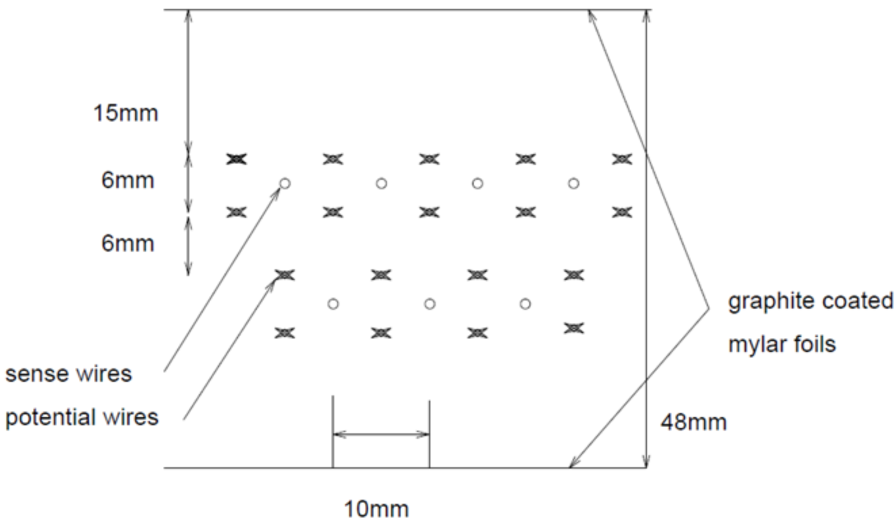

Figure 35: Drift cell geometry of the DCH.

To minimize multiple scattering effects, the wire chambers are constructed with minimal amount of material along the beam direction. A schematic view of the geometry of one view is shown in Fig.35. Sense wires have a diameter of 20 μm and made of gold-plated tungsten. The electric field is created by applying a negative voltage on two planes of gold-plated Ti-Cu wires located on each side of the sense wire planes, at a distance of 3 mm. The field wires have a diameter of 120 μm. The spacing between sense and field wires on a plane is 10 mm. Thin Mylar foils (22 μm) coated with graphite are used to shape the electric field in the drift cell and also to act as separating walls between two consecutive views.

A readout time measurement accuracy of about 1 ns with no deadtime is achievable with specially designed amplifiers and TDC circuits [17]. The anode signals in the wire chambers are amplified, discriminated and transformed to logic pulses in electronic circuits located on the chambers. The output pulse is a logic 50 ns wide ECL pulse with 50 ns deadtime following the pulse, achieved by a delay element.

The granularity of DCH is sufficient to perform measurements of interactions with light ions (up to Ar). The DCH wire occupancy in interactions of middle and heavy nuclei is too high to perform efficient track separation. Thus, the DCH will be replaced by cathode strip chambers (CSC) to perform track measurements in middle and heavy nucleus collisions.

10.2 CSC

The full configuration of the outer tracking system for heavy ion program will consist of four planes of 1129×1065 mm^2 CSC (cathode strip chamber) and two planes of 2190×1453 mm^2 CSC. The CSC detectors are situated outside the magnetic field with the aim to make precise link to the tracks, reconstructed in the GEM detectors inside the analyzing magnet. Tracks refined in CSC are used to improve particles momentum reconstruction and to find corresponding hits in the time-of-flight systems ToF400 and ToF700.

The first CSC detector with the size of the active area of 1129×1065 mm^2 was designed and assembled at LHEP JINR in 2018. It consists of an anode plane located between two cathode planes (see Fig. 36). The anode plane is a set of gilded tungsten wires with the diameter of 30 μm which are fixed on the plane with a step of 2.5 mm. The gap between the anode plane and each cathode plane is 3.8 mm. Two-coordinate readout of the signal is performed on two cathode PCB boards using sets of parallel metal strips. The inclination angles of the cathode strips to the vertical axis are 0 degrees (X coordinate) and 15 degrees (Y coordinate). The pitch of the X and Y strips is 2.5 mm. PCBs are glued to the support honeycomb. Due to a large multiplicity of charged particles in Au-Au collisions, readout layer is divided into outer (cold) and inner (hot) zones.

First beam tests of the 1129×1065 mm^2 CSC were performed in 2018 at the argon beam with kinetic energy of 3.2 AGeV and the krypton beam with kinetic energy of 2.3 AGeV at the Nuclotron. The CSC was installed upstream the ToF-400 time-of-flight detectors. The main goal of the tests was to study the performance of the CSC detector and the FEE and readout electronics as a part of the BM@N experimental setup. The signal clusters were reconstructed as groups of adjacent strips with amplitudes of signals above the threshold. For the reconstructed clusters, the center of gravity, the width and the total charge were calculated. The average cluster width is 6 strips which is equal to 15 mm. The gap size between the anode and cathode is reduced to 3 mm instead of 3.8 mm in order to improve the spatial resolution in multitrack events.

All four CSC detectors with the size of the active area of 1129×1065 mm^2 and one detector CSC with the size of 2190×1453 mm^2 were integrated into the BM@N setup in the physical run 2022-2023 with the Xenon beam at the kinetic energy of 3.8 AGeV at the Nuclotron

Two CSCs of the size 2190×1453 mm^2 have been designed to cover the ToF-700 system on both sides and replace the existing drift chambers (DCH). The design of these cathode strip chambers is shown in Fig. 37. One cathode plane consists of 8 PCBs, each PCB is divided into hot and cold zones. The hole in the center of the chamber is designed for the vacuum beam pipe. The gap size between the anode and cathodes is planned to be 3 mm. Two-coordinate readout of the signal is performed using sets of parallel metal strips with the inclination angle of 0 degrees for the X coordinate and 15 degrees for the Y coordinate. The pitch of the X and Y strips is 2.5 mm.

10.2.1 Front-end electronics

Front-end electronics is based on the same charge sensitive pre-amplifier chip VA163 as used for the GEM detectors. The multiplexed data from each board are transmitted through the twisted pair

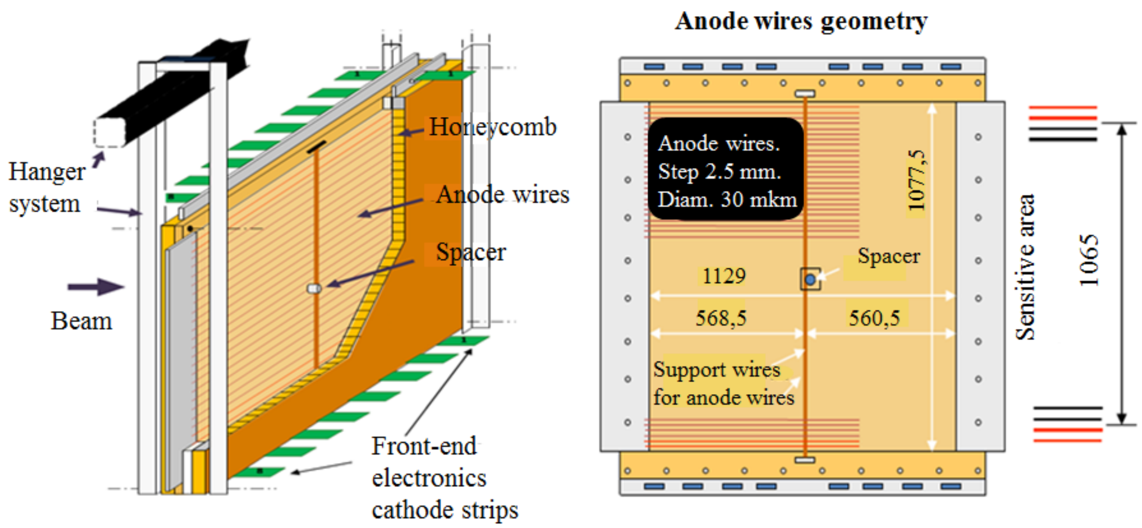

Figure 36: Schematic view of the 1129×1065 mm^2 CSC

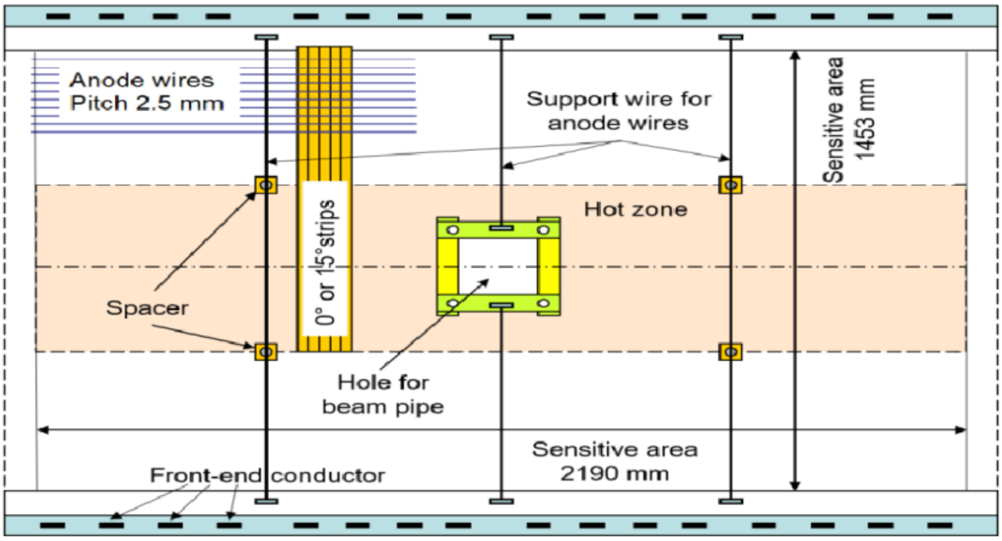

Figure 37: A technical drawing of the cathode strip chamber of the size 2190×1453 mm^2 (15-degree strips are not shown in this picture).

flat cable to the 12-bit analog-to-digital converter (ADC) readout by the BM@N data acquisition system.

The full configuration with 6 CSC detectors equipped with the electronics based on VA-163 chips (35000 readout channels) is planned to be integrated into the BM@N experimental setup at the 2023.

10.2.2 Gas distribution system

The outer tracker were operated with Ar(75%) + C_4H_{10}(25%) / C_3H_8O (vapor) gas mixtures. The gas system (Fig. 38) consists of two parts: 1) the mixer system which delivers a mixture of gases in a required ratio and pressure to downstream elements; 2) the distribution system, which delivers the gas in well defined quantities to the individual detectors.

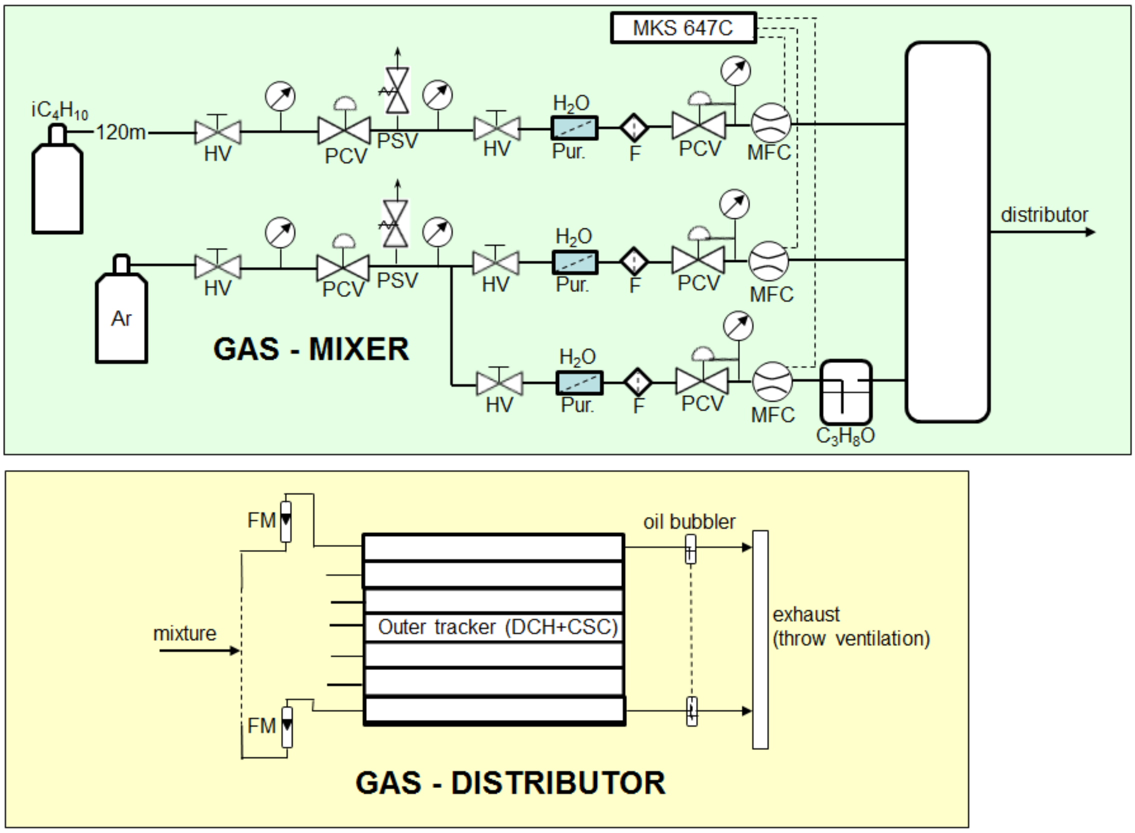

Figure 38: The gas line for the outer tracker. The layout of the mixer module: HV – on/off valve, PCV – pressure control (constant) valve, PSV – pressure safety valve, Pur. – Purifier (H2O and O2), F – filter, MFC – mass flow controller (MKS Instruments firm), MKS 647C – power supply and readout (MKS Instruments firm). Component layout of the distributor module: FM – flowmeter (manually flow adjustment), oil bubbler – pressure and air protection.

11 Forward Spectator Detectors

The new forward detectors for measuring the energy (FHCal) and charges (FQH, ScWall) of projectile spectators produced in the nucleus-nucleus collisions in the BM@N experiments have been developed and constructed during last few years. They are located at the very end of the BM@N facility (see Fig. 1). These detectors are used to determine the centrality and orientation of the reaction plane. Moreover, ScWall and FQH can be used also to study the charge distributions of spectator fragments produced in the nucleus-nucleus interactions. The rapidity coverage of these ~~forward detectors is shown in Fig.X1.~~

~~(fig.X1 - one picture for all detectors ?)~~

11.1 Forward Hadron Calorimeter (FHCal)

The forward hadron calorimeter FHCal has a granular structure in the transverse and longitudinal planes. It consists of 54 separate modules which provides transverse granularity of the FHCal. Internal part of the FHCal consists of 34 small modules with transverse sizes of 15×15cm^2 and a length equivalent to 4.0 nuclear interaction lengths. These modules are identical to the modules of the forward hadron calorimeters of the Multi-Purpose Detector (MPD) experiment at the NICA accelerator complex [8]. Two outer lateral parts of the calorimeter consist of 10 large modules on each side with transverse sizes of 20×20cm^2 and a length equivalent to 5.6 nuclear interaction lengths. These modules were initially constructed for the hadron calorimeter of the Compressed Baryonic Matter (CBM) experiment (FAIR, Darmstadt, Germany) [9] and are temporarily used in the hadron calorimeter of the BM@N experiment ~~in according with mutual agreement between BM@N and CBM collaborations~~. Schematic view of the FHCal is shown in Fig. 39, left. At the center of the calorimeter there is a hole with transverse size 15×15cm^2. Noninteracted beam ions pass to a beam dump located behind the calorimeter through this hole. It is necessary to protect internal modules of the calorimeter against high radiation dose and strong activation in experiments with heavy ion beams.

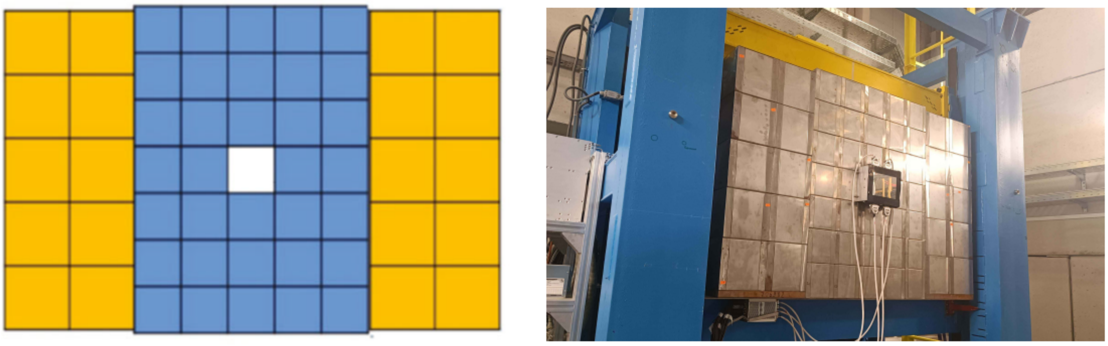

Figure 39: Schematic view of the FHCal, left. Photo of the FHCal with FQH installed on the the movable platform (blue) at the BM@N, right.

FHCal modules have sampling structure and consist of lead/scintillator layers with a sampling ratio of 4:1 (the thickness of the lead plates and scintillator tiles are 16 mm and 4 mm, respectively) and provide compensation condition (e/h=1) for the hadron calorimeter [??]. Small modules have 42 lead/scintillator layers and large modules have 60 such layers. To get rather hard rigidity of the lead plates they are made of lead-antimony alloy. An assembly of 60 (42) alternating layers of scintillator and lead plates are tightened into one package with a 0.5 mm thick stainless steel band using a special tensioning mechanism. The tape is welded with spot welding to the steel plates inserts installed in the beginning, middle and end of the package (Fig. 40). Behind the tightening mechanism the block of boron polystyrene with thickness 10 cm is installed in large modules. Once the package is assembled, it is closed by an upper box of 0.5 mm thick stainless steel sheet.

The scintillator plates are made from polystyrene-based plastic scintillators produced by Uniplast (Vladimir, Russia). Light from each scintillator plate is collected by wavelength shifting optical fiber KURARAY Y-11(200) glued into groove with depth 1.2 mm on the surface of the scintillation plate and transported to the end of module. The grooves in scintillators of large modules have circular form, while grooves in scintillators in small modules are spiral. Outside of the scintillator plate fibers are placed in thin black plastic pipes to be optically shielded and are stacked in parallel on the top surface of the module package. All scintillators with glued fibers are wrapped in Tyvek reflector.

The end of each fiber glued in the scintillator plate is coated with reflective paint. At the end of the module the optical fibers from each of the six consecutive scintillation plates in the module are glued into individual optical connectors, which are placed on a panel mounted in the module box. Thus, each of large modules has ten longitudinal sections and each of small modules has seven sections. The longitudinal segmentation provides high homogeneity of light collection along modules, a large dynamic range of the calorimeter response and makes it possible to perform energy calibration of FHCal with cosmic muons [10].

This panel with ten optical connectors for large module (seven optical connectors for small module) has an additional optical connector for LED light distribution system. LED pulses are distributed with ten (seven) optical fibers into each section optical connector. Light pulses from the LED allow to control the operation of the photodetectors used for light readout.

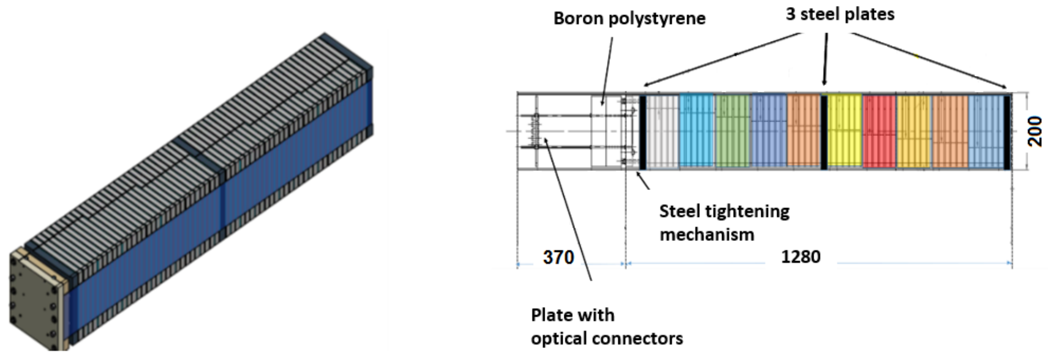

Figure 40: Left - 3D view of the large calorimeter module in assembly. Right - scheme of large module, here 10 sections are shown in different colors.

The weight of each small module is about 200 kg and weight of large module is about 500 kg. Total weight of the FHCal is about 17 tons. It is mounted on the special platform shown in blue color on Fig. 39, right, which is able to move FHCal in X-Y directions.

11.1.1 FHCal photodetectors, FEE and readout electronics

~~At present,~~ Hamamatsu MPPC S12572-010P with 3×3mm^2 sensitive area are used as photodetectors for light detection from the sections of the FHCal. These photodetectors have gain 1.35×10^5 and photon detection efficiency about 10% at peak sensitivity wavelength 470 nm. Due to very small pixel pitch - 10mkm - the total number of pixels is 90000 which is important to provide the linear response in wide dynamic range of the signal. FHCal Front-end-electronics (FEE) is composed of two separate PCBs. Ten (seven) photodetectors are installed on a first PCB directly connected with light connectors at the end of each large (small) module, ~~Fig. ??, left.~~ A temperature sensor is mounted near photodetectors on aluminum heat sink. The second PCB contains signal preamplifiers with differential ADC driver output and individually adjustable voltage regulation circuits for the photodetectors, ~~Fig. ??, center.~~ This board has also LED flash generation circuit with synchronization input and analog sum signal output. All FEE boards are remotely controlled via specially designed HVSys System Module manufactured in JINR (Dubna, Russia).

There are 438 calorimeter sections, which are needed to be readout. Eight ADC64s2 [??] boards, produced at JINR (Dubna, Russia) are used for signal readout. They have 64 channel 12-bit ADCs with sampling rate of 62.5 MHz and memory depth of up to 1024 points per channel. The ADC64s2 boards have Lemo connectors for trigger and Xoff signals, and are capable of time synchronization via White Rabbit network, providing per-channel zero suppression function with adjustable threshold and can operate in self-triggered or externally triggered modes. FHCal ADCs are fully integrated into the BM@N data acquisition system which provides trigger signals, busy logic, White Rabbit network and data readout. Power for FHCal ADCs is provided by a remotely controlled power supply units placed in Wiener crate.

Custom 12-channel analog sum modules (adders) with individually adjustable attenuation have been constructed. These adders are used to sum up the analog outputs from FHCal modules. They are used when performing standalone cosmic calibrations in central DAQ. The adders can be used for integration into the BM@N trigger system.

11.1.2 FHCal calibration with cosmic muons, energy resolution and linearity of the response

Since muon beams are unavailable at the BM@N setup, energy calibration of the FHCal can only be performed using cosmic particles. Longitudinal and transverse segmentation of the calorimeter allows for track reconstruction [10], which was used to compensate for track length variation in the scintillator tiles due to varying track orientation of the cosmic particles. Cosmic calibrations parameters show 40 - 50 photoelectrons per one muon per one section.

A detailed study of the linearity of response and energy resolution for array of 9 large modules has been performed on protons with kinetic energy range 1 - 9 GeV at the CERN T9 and T10 beamlines [11]. The good linearity and 0.54/sqrt(E) energy resolution was obtained.

11.2 Forward Quartz Hodoscope (FQH)

The FHCal beam hole is covered with beam hodoscope - Forward Quartz Hodoscope (FQH). The main goal of the FQH is measuring charges of spectator fragments which miss the calorimeter in order to estimate the collision centrality with combined FHCal and hodoscope response. The FQH consists of 16 strips - cherenkov detectors - with sizes of $16 \times 1 \times 0.4 cm^3$ (see Fig. 41, left) inside light tight box. Each FQH detector has light readout with two individual silicon photo-multipliers mounted on opposite sides of the strip (see Fig. 41, right).

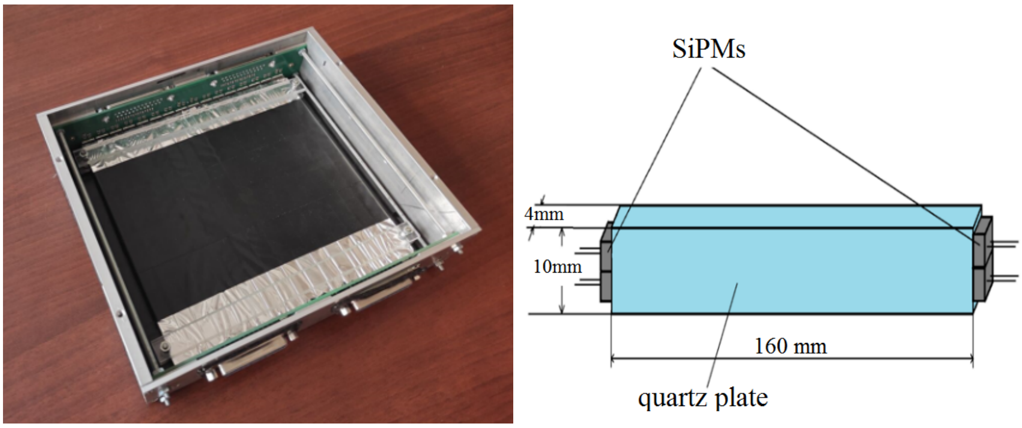

Figure 41: Left: photo of Forward Quartz Hodoscope - FQH (inside view). Right: picture of the FQH strip with SiPM photodetectors mounted.

One Front-End-Electronic (FEE) board reads eight channels. Total number of FEEs are four for full FQH. The FQH installed in front of the beam hole of FHCal is shown in Fig. 39 (right). Four FEE boards of FQH are connected to the control box with amplifiers installed at bottom side of FHCal.

Hamamatsu MPPCs S14160-3015PS with 3x3 mm2 sensitive area and PDE of 32% are used as photodetectors. Four TQDC-16 boards [?] with total 64 channels are used to read-out the two-gain outputs from each photodetector. The gains are 1x and 4x. Low gain channel is used for maximum dynamic range up to the highest ion charge expected. High gain channel is used for low-Z fragments. Charge calibration of FQH strips is performed with pure beam ions.

11.3 Scintillation Wall (ScWall)

The ScWall is the large area detector aimed for measuring the charged particles in forward rapidity. It consists of array of scintillating plates placed in the aluminum box. The polistirol-based scintillators are manufactured at "Uniplast" (Vladimir, Russia). ~~There are two sizes of scintillators: big cells of $15 \times 15 \times 1 cm^3$ at peripheral area and small ones of $7.5 \times 7.5 \times 1 cm^3$ in the central part. The view of the ScWall is shown in Fig. 42. The full detector size is $270 \times 120 cm^2$. The ScWall has 40 inner small cells and 138 big outer cells. In order to avoid heavy-ion beam radiation damage the very central part has $15 \times 15 cm^2$ beam hole (see Fig. 42).~~

The light in the cells is collected by WLS Y11(200) S-type (Kuraray) [?] fibers mounted in 1.5mm deep grooves (see Fig. 43) and detected by SiPM Hamamatsu S13360-1325CS with $1.3 \times 1.3 mm^2$ active area, gain of 7×10^5 and PDE of 25%. The measured light yields of big cells and small cells are about 32 p.e./MIP and about 55 p.e./MIP, respectively [?]. The full area of ScWall is divided into 12 read-out zones and performed with ADC64s2 board combined with FEE

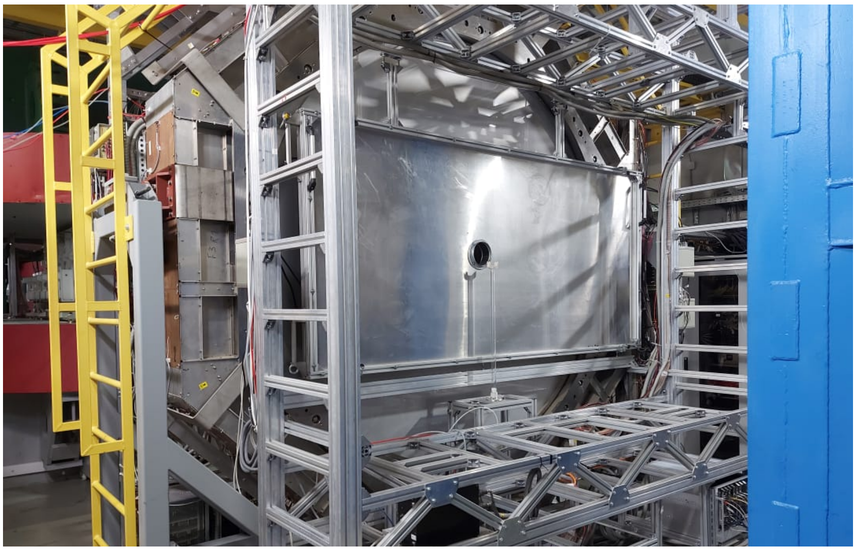

Figure 42: The view of ScWall detector with the beam hole.

boards. Three ADC64s2+FEE boxes are used for read full ScWall. The calibration of ScWall cells has been performed on cosmic muons as well as on Z=1 charge particles coming from the ion-ion reaction.

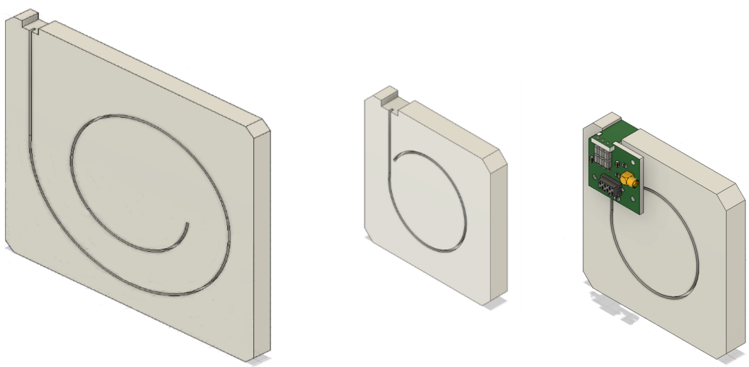

Figure 43: From the left to the right: schematic view of large ScWall cell, schematic view of small ScWall cell, schematic view of small cell assembly with SiPM on PCB board with connectors.

11.4 Slow Control for forward detectors

The FHCal, FQH and ScWall have SiPMs as light detectors. In order to control and monitor bias voltage (HV) applied to SiPMs and the temperature the new Slow Control system has been developed. The hardware part of Slow Control is designed and constructed by "HVsys" (JINR, Dubna). HV power supply modules have multi-channel HV supplies with micro-controller interface. Schematic view of Slow Control system is shown in Fig. 44. Each HVsys system module has a unique IP-address for communication through individual proxy-server. Communication of HVsys box with FEE micro-controllers is done with RS-485 interface. All proxy-servers have connections to GUI panel to control and monitor status and to perform temperature correction for all SiPMs. The software part of the Slow Control is written on python3 [12].

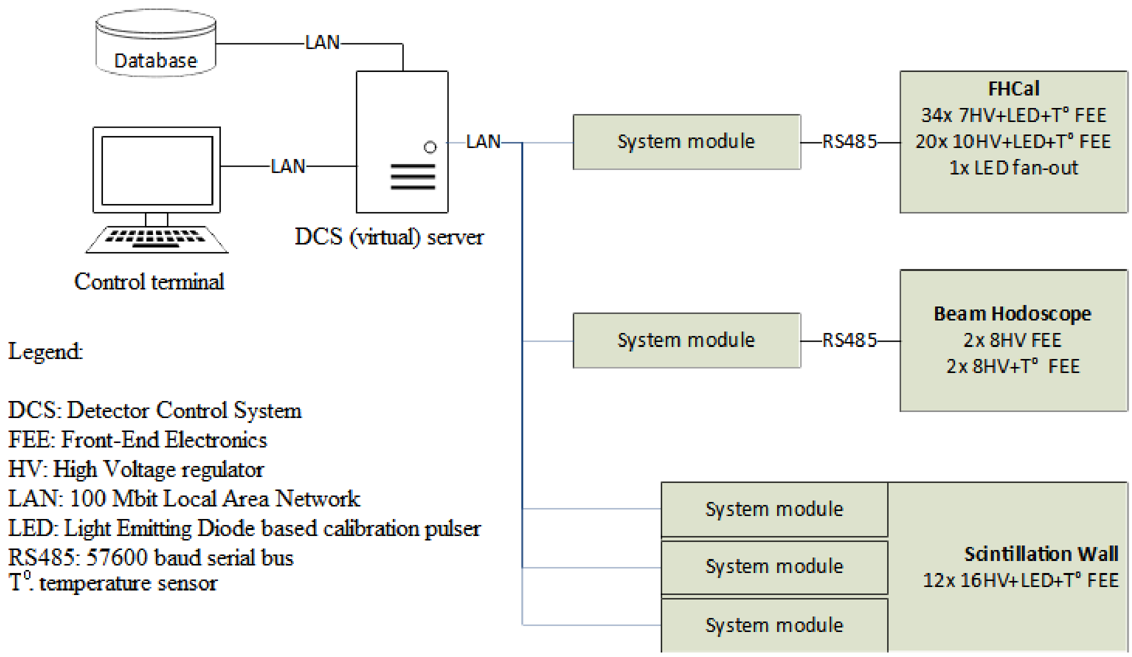

Figure 44: The Slow Control system for forward detectors at BM@N.

12 Trigger

BM@N trigger consists of hardware and sofware parts. The hardware part includes detectors on fast plastic scintillators, low- and high- voltage power suppliers, programmable trigger logic unit T0U, trigger control unit CAEN N6742. The software part include a graphic trigger interface, trigger performance and beam quality control.

A beam trigger BT formed by the signal coincidence from beam couters BC1, BC2 under condition the signal absence from the veto counter VC:

$$BT = BC1 \times BC2 \times VC(veto)$$

A minimum bias trigger MBT asks only for a low amplitude signals in forward counter FD, which corresponds to the beam particle interaction in a space between BC2 and FD counters:

$$MBT = BT \times FD(veto)$$

The interaction trigger called Central Collision Trigger (CCT) composed of the minimum bias trigger and the multiplicity in the barrel detector:

$$CCT = MBT \times BD(> N)$$

All the triggers mentioned above (BT, MBT, CCT) are send in the output data stream with the corresponding scaling factor.

Trigger decision formed by the programmable logic controller T0U and its logic organisation is shown in Fig. 45.

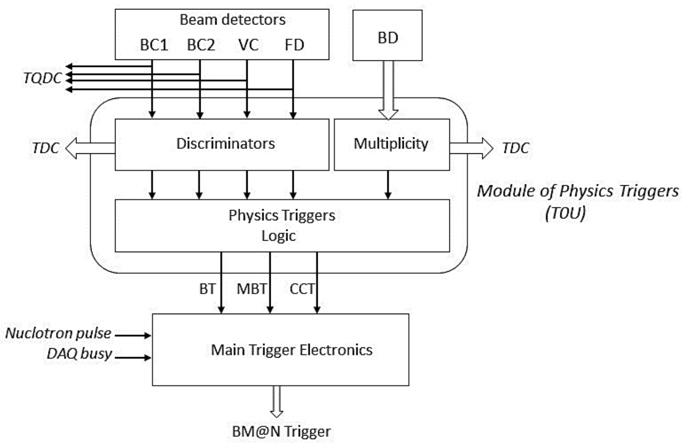

Figure 45: Trigger logic.

13 BM@N DAQ: Hardware Architecture

The core function of the DAQ system is realization of data transfer from the detector to the storage system. It includes the data flow from readout electronics to the First Level Processor (FLP) fabric, to the Event Building (EB) and to the Storage System. Main DAQ components are readout electronics modules, clock and time synchronization system, trigger distribution system, data transfer networks, data processing servers and online storage system ($\_link - to - tdr\_$). The general architecture is sketched in Fig. 46.

Detector Readout Electronics (DRE) boards record detector signals. There are two main types of DRE boards grouped by function: Timestamping Time to Digital Converters (TDC), Waveform Digitizers or Amplitude to Digital Converters (ADC).

13.1 TDC DRE board

TDC DRE board performs time-stamping of discrete signals (hits) with typical accuracy of $20ps$. It is based on HPTDC chip. Hit timestamps are kept for $51\mu s$ in ring type memory. The total trigger latency should not exceed this value. ADC DRE board is a waveform digitizer. It quantize analogue input signal and samples it at fixed time intervals. Zero suppression logic is based on baseline estimation and threshold value. Signal shaping can be performed in digital form with FIR filters. It allows to reduce the number of waveform points required for digital signal representation with minimum loss of accuracy. The ring type memory allows the read back of last $32\mu s$ of waveforms. It sets the limit on trigger latency to this value. TQDC DRE board combines both TDC and ADC functions.

13.2 MSC16VE module

MSC16VE is 16-channel multievent scaler (Fig. 48). Each channel input has 50Ω impedance and accept signals of ±2.5V range and discrimination threshold can be adjusted in ± 1V range. Module has 4 LVTTL count enable (CE) inputs. Ethernet 1000BASE-X connection is used for data readout and module control. Module MSC16VE has three main logic parts: input part, multi-event data readout and hardware histograms. Input part has crosspoint switch that allows any input channel to be processed by any multi-event counter and histogram. CE and Gate logics have 16 independent Look-Up Tables (LUT) each. Gate logic determines reset conditions for hardware histograms. Multi-event counters data continuously splits into numbered time slices and pushes to data encoder and further to Ethernet. Time slices length is adjustable with minimum length of 64 ns and 8 ns step. Data encoder perform zero suppression and data packing. Hardware histograms are used for online monitoring of input hits. Time series histograms store hits distribution in time. Time interval histograms store time interval between two adjacent hits in channel. Both hardware histograms readout by request from control software.

13.3 Timing System

White Rabbit provides sub-nanosecond accuracy and picosecond precision of time synchronization for distributed systems. DRE boards digitize detector signals using common notion of time and frequency provided by the White Rabbit (WR) network. The time reference is provided by GPS/GLONASS receiver and backup precision frequency reference (Rubidium clock). Digitizer boards require precise reference clock for high precision measurements. Timestamping TDCs used in T0, TOF400, TOF700 detector electronics have time resolution of $25ps$, DCH-$100ps$. DRE boards include White Rabbit Node Core and tunable crystal oscillators that are synchronized to reference clock with $10ps$ accuracy. WR node core provides local clock and timestamp at 125 MHz. The timestamp is specified as TAI (International Atomic Time). It is an absolute number of seconds and nanoseconds since 01.01.1970. Frequency dividers synchronized by 1 PPS (Pulse per Second) signal are used to produce digitizer clocks: 41.667 MHz for HPTDC ASICs and 62.5 MHz for waveform digitizers.

13.4 Trigger distribution system

BM@N trigger system has tree structure and 3 trigger levels: L0, L1 and L2.

13.4.1 General architecture of trigger distribution system

L0 is fast trigger signal for front-end electronics with latency of $150ns$. L1 trigger signal is readout trigger candidate generated by TRC module (see 13.4.2), according to its internal logic. Formation time of L1 trigger is adjustable and was $\tilde{1}\mu s$ in BM@N run 8. L2 trigger, produced by UT24VE module (see 13.4.3), starts data readout for all subsystems. All signals are transmitted via coaxial cables in LVTTL standard. Trigger-Busy handshake algorithm for L2 trigger was implemented to guaranty all triggers delivery to all subsystem. This algorithm is shown in the Fig. 49. Rising edge of trigger signal (1) leads to rising edge of busy signal (2). After that trigger signal is deasserted (3). Upon completion of data collection, the subsystems deassert busy signals (4). Typical subsystems busy time shown in the Fig. 50.

13.4.2 TRC – Trigger Control

TRC (TRigger Control) module was designed for BM@N run 8. Main goal of this module is production of readout trigger candidates (L1) according to its configurable logic. T0 unit is used as source for input signals ("physical" triggers BT, CCT, MBT, etc.). Each of 16 input channels has individual settings: input delay, hits downscaling factor and before/after protection. Before/after protection logic used for pile-up rejection and secondary hits rejection during detectors dead time. L1 trigger candidate output delay can be adjusted in range of 8 ns to 100 μs. TRC module produces L0 trigger for GEM, CSC, FSD and BT front end electronics, as they required fast (less then 300 ns) data latch signal. Different conditional counters for input physical triggers are implemented in TRC module.

13.4.3 LTU - Logical Trigger Unit

LTU is main module for L2 trigger generation and distribution system. The module ensures the operation of Trigger-Busy handshake algorithm (Fig. 49) and can process up to 16 busy channels. Busy signals can be received from DRE modules or hierarchically lower LTU modules. Time intervals between accepted triggers and busy signals duration are histogramed in LTU internal memory. Various trigger counters are also implemented in module.

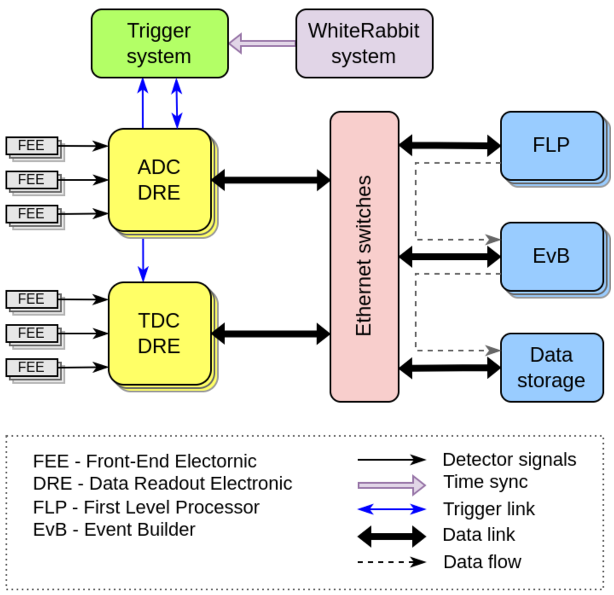

Figure 46: General architecture of DAQ system

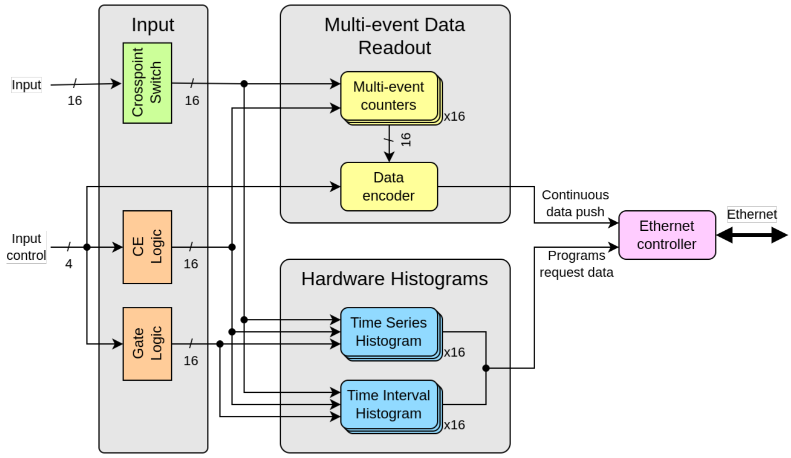

Figure 47: MSC16VE module.

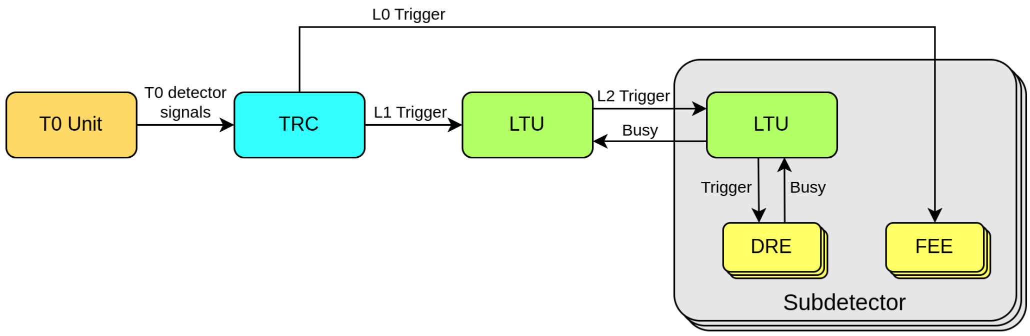

Figure 48: BM@N trigger architecture.

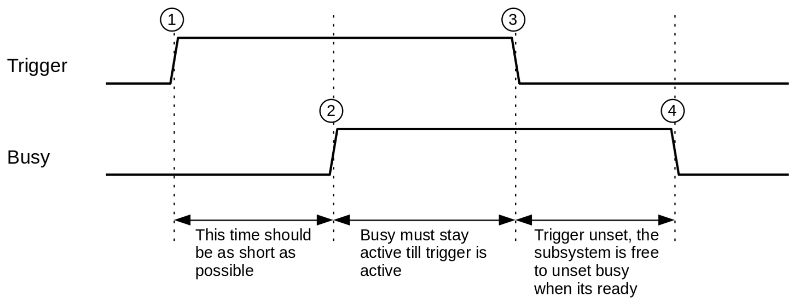

Figure 49: Trigger handshake chronogram.

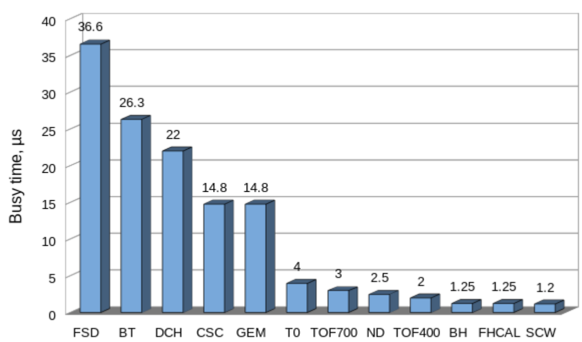

Figure 50: The average busy time for all subsystems.

13.5 DAQ data flow

All BM@N subdetectors except DCH use Ethernet to transfer data from readout electronics to First Level Processors. Primary FLP task is to receive data stream in real time, buffer, validate, format and enqueue data blocks to event building network. FLP decouples fast microsecond-scale synchronous data acquisition process from slower seconds-scale software data processing by buffering data in computer RAM. Data transfer path from readout electronic module to event building network and storage system is shown on Fig. 51 for typical 64-channel ADC based waveform digitizer module ADC64VE.

Electronic modules designed by DAQ team share common communication architecture. Network connectivity is provided by hardware IP stack (HWIP), a programmable logic code synthesized for onboard FPGA processor. Taking into account limited memory and logic resources of FPGA chips available, and implementation complexity of TCP protocol, custom data transfer protocol MStream has been designed for data streaming over 1 Gb/s or 10 Gb/s Ethernet networks. It uses UDP over IP as transport layer, and implements ordered and reliable data packet delivery using acknowledgments.

FLP receive data stream in real time. Dedicated servers with dual 18-core CPUs, equipped with dual 100 Gb/s Ethernet adaptors, are running Fedora-36 Linux OS. Tuning for real-time operation is necessary to ensure continuous data transferred without interruptions [18]. It includes CPU frequency and supply voltage management, network adapter interrupt coalescence mitigation and system task scheduler adjustments.

BM@N readout electronics deliver 6 GB/s of raw data over 200 streams in peak at 10 kHz trigger rate. Single data stream has 500 MB/s maximum sustained throughput when using 10 Gb/s Ethernet. Run 8 operation has shown that single manually tuned FLP server is capable of hosting 10-12 data stream receivers with minimal contribution to overall busy time.

Software event building in BM@N is part of asynchronous processing, it does not affect readout busy time under normal operation. Event builders are cascaded in multiple layers for load distribution, and last layer writes data files to storage system.

Event Builder programs associated with data intensive subdetectors run on dedicated hardware servers, while event builders for low data rate subdetectors run in KVM virtual environment, as well as readout control programs. It allows to utilise computer resources efficiently.

13.6 DAQ storage system

DAQ storage system is comprised of 10 servers with NVMe solid state devices for low latency I/O operations and 12 servers with hard disks for high volume storage. It is distributed software defined object storage cluster under control of Ceph software ([19]). Cluster management and interface functions are implemented on 6 dedicated single-CPU servers. Configurable 'CRUSH map' algorithm defines data object to storage device mapping. Ceph cluster has self recovery functions and it performs periodic data read check on regular intervals to ensure data integrity. It is highly available and reliable system with no single point of failure.

Storage devices are organised in pools with different data redundancy algorithms. Pools allocated on NVMe devices have triple replication provide 100 TB usable space, and are used as block storage for virtual machine cluster. Hard disk pool has 2.2 PB usable capacity. It use erasure coding replication with 40% overhead. POSIX compatible filesystem interface CephFS is used for experimental data storage. Server hardware characteristics are shown in Table 8.

Qty	Function	Specifications	Network
20	Compute node	Dual 18-core 3 GHz CPU, 384 GB RAM	Dual 100 Gb/s
10	NVMe storage server	$10 \times$ 3.5TBNVMe	Dual 100 Gb/s
8	HDD storage server 1	$24 \times$ 12TBHDD, 1.8TBSSDcache	Dual 100 Gb/s
4	HDD storage server 2	$24 \times$ 18TBHDD, 3TBSSDcache	Dual 100 Gb/s
6	Control server	4-core CPU, 64 GB RAM	Dual 25 Gb/s
1	Bootstrap server	4-core CPU, 16 GB RAM, $4 \times$ 300GBHDD	Dual 1 Gb/s

Table 8: Characteristics of BMN DAQ server equipment.

13.7 Virtual computing cluster

Programs performing readout control functions, detector slow control, software and infrastructure monitoring and other services are run on KVM virtual machines or LXC containers that reside on highly available cluster. Approx. 100 virtual machines in total reside on 10 compute nodes. Cluster has backup and snapshot rollback mechanisms that are necessary for safe software administration and recovery in case of errors. Virtual cluster is also used as offline computing farm for batch and interactive analysis when no data taking is in progress.

13.8 BM@N DAQ IT Infrastructure

DAQ server equipment is located in 4 racks in MDC (modular data center), Fig. 53 49 servers occupy 81 units of rack space in total. Table ?? shows server types and functions.

Virtual machine cluster is comprised of 10 compute nodes running Proxmox VE version 7 software. Other 10 compute nodes are dedicated servers for FLP and event builders and run Fedora-36 OS. Storage servers run CentOS 8 Stream OS.

Basic network infrastructure services (RADIUS, DHCP, DNS) are provided by virtual cluster with redundancy. During cold startup, while virtual cluster is not yet ready, basic services are provided by bootstrap server. By design DAQ system is not dependant on any external network or software services and autonomous operation is possible.

Core of data network is two-level Ethernet fabric with Clos architecture that has two switches on spine level and multiple switches on leaf level Fig. 52. Ethernet VPN (EVPN) virtualisation technology is used to allow flexible traffic management, high availability and efficient link utilisation. Underlay network provide connectivity between fabric nodes, it is formed by leaf and spine switches connected with L3 routed links, topology is managed by OSPF dynamic routing protocol. Overlay network that carry user traffic is realised with MP-BGP protocol at control plane and VXLAN encapsulation at data plane.

DAQ network supports jumbo ethernet frames up to 9000 bytes to maximise throughput of data transfer from readout electronics. Network supports Any-Source Multicast that is necessary for automatic discovery of readout electronics modules and software components of distributed DAQ system.

Two spine and four leaf switches are located in racks of MDC. Other leaf switches and access switches of slow control systems are located in electronics racks in experimental area. Two core routers of DAQ technological network are located in building 201 and provide connectivity to campus network with 200 Gb/s bandwidth.

Compute and storage servers, readout electronics and additional level of 1 Gb/s access switches for slow control systems are connected to fabric leaf switches. Critical components have dual connections to pairs of leaf switches for high availability using LACP link aggregation protocol.

DAQ network has shown no critical problems during BMN data taking Run 8. Ethernet switching fabric bandwidth is adequate for peak traffic conditions and has no negative impact on data taking performance. No significant packet drops or errors were registered by monitoring system on network fabric switches that could indicate network saturation and packet buffer overflows. Considering both trigger rate and event size increase on next data taking run, it is possible to double fabric bandwidth by additional leaf to spine connections.

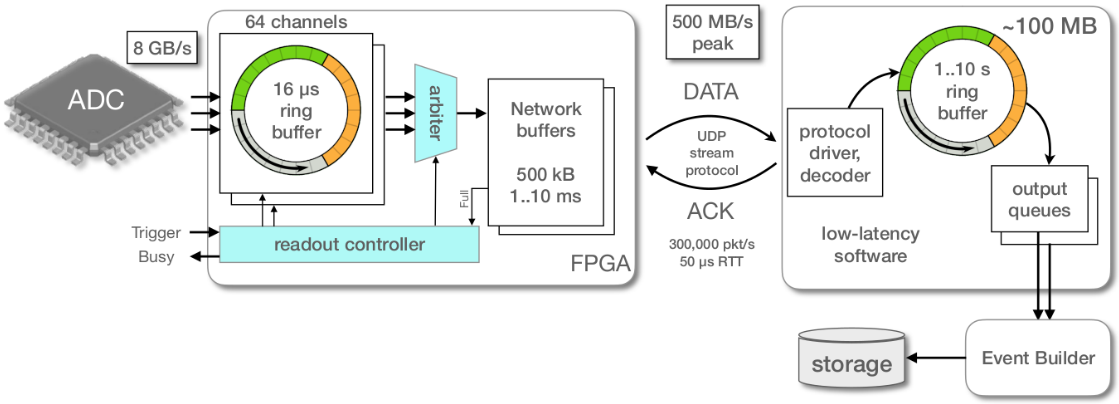

Figure 51: Data transfer from detector to storage system.

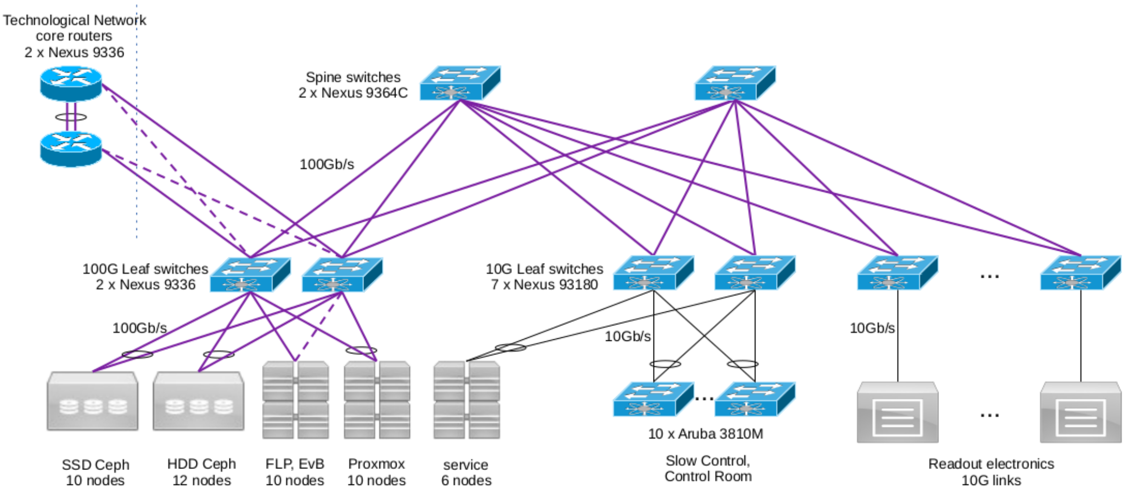

Figure 52: BMN DAQ Network.

Figure 53: BM@N Modular Data Center server racks.

14 Slow Control System

Main objectives of Slow Control System (SCS) include hardware status monitoring, archiving the operational properties of the facility, user-friendly graphical interface and alarm management system. The SCS was built around “TANGO Controls”[20] - an open-source toolkit, widely used in scientific experiments.

Slow Control data from experiment subdetectors such as: high voltage, low voltage, vacuum, gas flow and mixture etc. are aggregated by SCS. Those are then stored in the “historical database” - a PostgreSQL database with TimescaleDB extension[21]. It is implemented as distributed cluster with backup and load balancing

The user interface for live monitoring and retrieving past data is developed with Grafana[22] – an open-source analytics and interactive visualization web application. A mnemonic scheme of the experiment displaying hardware status and alarms (Fig. 54) was also implemented with it.

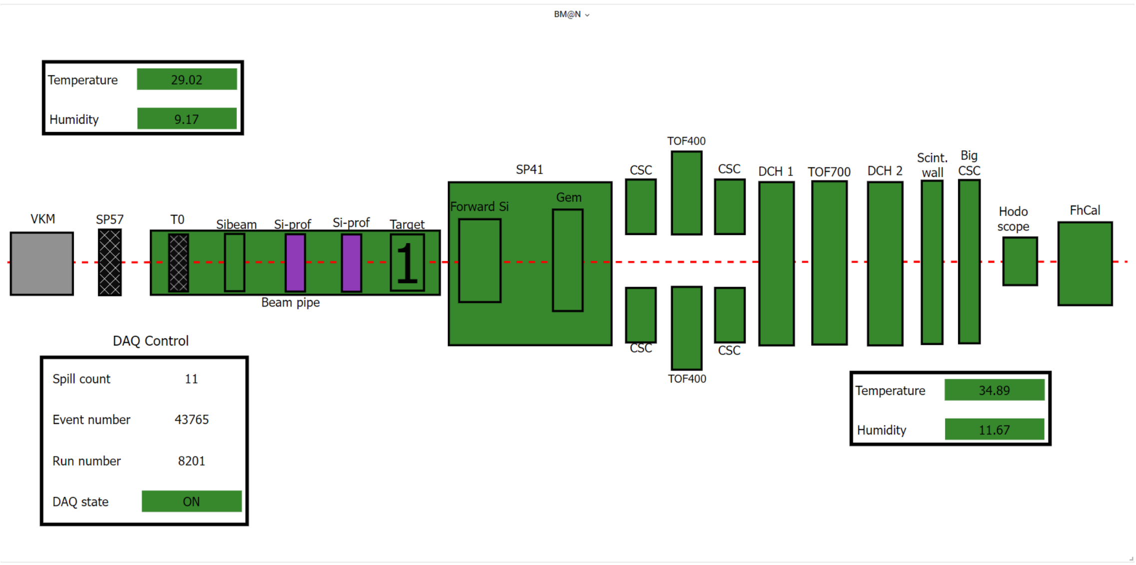

Figure 54: Slow Control System Main View.

TANGO Database, hosting the configuration of the whole system, and TANGO Historical Database are running on the BM@N virtual machine cluster. While programs, controlling and/or monitoring real hardware are running either on virtual cluster or on dedicated PCs of different subdetectors.

15 Summary

The detailed description of BM@N spectrometer is given. In this configuration t the fall of 2022 and the beginning of 2023 a big data set was recorded during 3 moths period. About 500M events with the different trigger condition are available for a physical analysis. A preliminary ananlysis of about 1% of data shows a signals particles decays with strange quarks (K^0_S, Λ). The signature of charge pions, kaons and protons is visible if the time flight system TOF400/TOF700 is involved in the data analysis. The resolution in particle momentum, the width of the invariant mass distributions are in agreement with the expected values estimated by MC simulation. The BM@N collaboration acknowledges the efforts of the staff of the accelerator division of the Laboratory of High Energy Physics at JINR that made the data taking possible and successful. The BM@N collaboration acknowledges support .....

References

[1] M. Kapishin (for the BM@N Collaboration), Eur. Phys. J. A52 (2016) no. 8, 213.

[2] J. Randrup and J. Cleymans, Phys. Rev. C 74 (2006) 047901.

[3] B. Friman, W. Nörenberg, and V.D. Toneev, Eur. Phys. J. A 3 (1998).

[4] NICA White Paper, Eur. Phys. J. A 52 (2016).

[5] BM@N Conceptual Design Report: http://nica.jinr.ru/files/BM@N/BMN_CDR.pdf

[6] Ch. Fuchs, Prog. Part. Nucl. Phys. 56 (2006) 1-103.

[7] P. G. Akishin *et al.* Optimization of a Large Aperture Dipole Magnet for Baryonic Matter Studies at Nuclotron, Phys. Part. Nucl. Lett. 2015. V. 12. P. 305

[8] A. Ivashkin *et al.* http://mpd.jinr.ru/doc/mpd-tdr/ 2017

[9] F. Guber *et al.* http://repository.gsi.de/record/109059/files/20150720 2015

[10] A. Izvestnyy, N. Karpushkin, F. Guber, S. Morozov and O. Petukhov, Calibration of FHCal with cosmic muons at the BM@N experiment, J. Phys. Conf. Ser. 1690 (2020) no.1, 012060.

[11] N. Karpushkin *et al.* Study of the hadron calorimeters response for CBM and BM@N experiments at hadron beams, J. Phys. Conf. Ser., 2020. 2̌0132̌013 Vol. 1667, no. 1. P012020. DOI: 10.1088/17426596/1667/1/012020.

[12] O. Petukhov, S. Morozov, Development of Detector Control System (DCS) for forward hadron calorimeters in the BM@N and the MPD experiments, J.Phys.Conf.Ser. 1690 (2020) 1, 012063, DOI: 10.1088/1742-6596/1690/1/012063

[13] D. Baranov *et al.* GEM tracking system of the BM@N experiment, 2017 JINST 12 C06041. DOI 10.1088/1748-0221/12/06/C06041.

[14] A. Galavanov *et al.* Status of the GEM/CSC tracking system of the BM@N experiment, 2020 JINST 15 C09038. DOI 10.1088/1748-0221/15/09/C09038.

[15] A. Galavanov *et al.* Performance of the BM@N GEM/CSC tracking system at the Nuclotron beam, 2019 EPJ Web Conf. 204 07009, https://doi.org/10.1051/epjconf/201920407009 .

[16] D. Bederede *et al.* Nucl. Instr. and Meth. A 367 (1995) 88.

[17] I. Augustin *et al.* Nucl. Instr. and Meth. A 403 (1998) 472.

[18] RedHat. Optimizing RHEL 9 for Real Time for low latency operation.
$(https://access.redhat.com/documentation/en-us/red_hat_enterprise_linux_for_real_time/9)$

[19] S. Weil et al. Ceph: A Scalable, High-Performance Distributed File System. OSDI 2̌01906: 7th USENIX Symposium on Operating Systems Design and Implementation.
$(https://ceph.com/assets/pdfs/weil-ceph-osdi06.pdf)$

[20] Tango is an Open Source solution for SCADA and DCS.
$(https://www.tango-controls.org/)$

[21] PostgreSQL is a powerful, open source object-relational database.
$(https://www.postgresql.org/)$

[22] Grafana is a multi-platform open source analytics and interactive visualization web application.
$(https://grafana.com/)$